

# Implicit Data-Driven Regularization in Deep Neural Networks under SGD

Meng Xuran, Yao Jianfeng

*Department of Statistics and Actuarial Science, University of Hong Kong,  
Hong Kong SAR, China*

*\*To whom correspondence should be addressed: jeffyao@hku.hk*

## Abstract

Much research effort has been devoted to explaining the success of deep learning. Random Matrix Theory (RMT) provides an emerging way to this end: spectral analysis of large random matrices involved in a trained deep neural network (DNN) such as weight matrices or Hessian matrices with respect to the stochastic gradient descent algorithm. In this paper, we conduct extensive experiments on weight matrices in different modules, e.g., layers, networks and data sets, to analyze the evolution of their spectra. We find that these spectra can be classified into three main types: Marčenko-Pastur spectrum (MP), Marčenko-Pastur spectrum with few bleeding outliers (MPB), and Heavy tailed spectrum (HT). Moreover, these discovered spectra are directly connected to the degree of regularization in the DNN. We argue that the degree of regularization depends on the quality of data fed to the DNN, namely Data-Driven Regularization. These findings are validated in several NNs, using Gaussian synthetic data and real data sets (MNIST and CIFAR10). Finally, we propose a spectral criterion and construct an early stopping procedure when the NN is found highly regularized without test data by using the connection between the spectra types and the degrees of regularization. Such early stopped DNNs avoid unnecessary extra training while preserving a much comparable generalization ability.

**Key words:** Deep Learning; Random Matrix Theory; Data-Driven Regularization; Early stopping

# 1 Background

In the past decade, deep learning (LeCun et al., 2015) has achieved impressive success in numerous areas. Much research effort has been since concentrated on providing a rational explanation of the success. The task is difficult, particularly because the training of most successful deep neural networks (DNNs) relies on a collection of expert choices that determine the final structure of the DNNs. These expert choices include nonlinear activation, hidden layer architecture, loss function, back propagation algorithm and canonical datasets. Unfortunately, these empirical choices usually bring non-linearity into the model, and nonconvexity of optimization into the training process. As a matter of consequence, practitioners of deep learning are facing certain lack of general guidelines about the “right choices” to design and train an effective DNN for their own machine learning problem.

To make progress on the understanding of existing trained and successful DNNs, it is important to explore their properties in some principled way. To this end, a popular way has recently emerged in the literature, namely spectral analysis of various large characteristic random matrices of the DNNs, such as the Hessian matrices of the back-propagation algorithm, weight matrices between different layers, and covariance matrices of output features. Actually, such spectral analysis helps to gain insights into the behavior of DNNs, and many researchers believe that these spectral properties, once better understood, will provide clues to improvements in deep learning training (Dauphin et al., 2014; Pappayan, 2019a,b; Sagun et al., 2017; Yao et al., 2020; Granzio, 2020; Pennington and Worah, 2019; Ge et al., 2021). Recently, Martin and Mahoney (2021) studied the empirical spectra distributions (ESD) of weight matrices in different neural networks, and observed a “Phase Transition 5+1” phenomenon in these ESDs. Interestingly, the phenomenon highlights signatures of traditionally regularized statistical models even though there is no set-up of any traditional regularization in the DNNs. Here, traditional regularization refers to the minimization of an explicitly defined and penalized loss function of the form  $L(\theta) + \alpha \cdot p(\theta)$  with some tuning parameter  $\alpha$  ( $\theta$  denotes all the parameters in the DNN). However, those well-known expert choices such as early stopping also produces a regularization effect in DNNs, and this is the reason why such expert choices are recommended for practitioners. Actually, Kukacka et al. (2017) presented about 50 different regularization techniques which may improve DNN’s generalization. Among them, batch normalization, early stopping, dropout, and weight decay are a few commonly used ones.

A main finding from Martin and Mahoney (2021) is that the effects of these regularization practices can be identified through the spectra of different weight matrices of a DNN. Moreover, the forms of these spectra in the “5+1 phase transition” help assess different degrees of regularization in the DNN. For instance, if these spectra are far away from the Marčenko-Pauster (MP) law, or the largest eigenvalue departs from the

Tracy-Widom (TW) Law (see in Appendix B), there is strong evidence for the onset of more regular structures in the weight matrices. A connection between implicit regularization in a DNN and the forms of the spectra of its weight matrices is thus established. Particularly, they considered the evolution of weight matrices spectra during the training process of a DNN from its start to its final stage (usually 200-400 epochs). The "Phase Transition 5+1" phenomenon precisely means the evolution during training dynamics.

However, [Martin and Mahoney](#) does not provide much insight on the fundamental factors that may drive and determine the observed form of the terminal spectra. At the final stage of the training, spectra can vary from Heavy Tail (HT) to MP law with spikes in different real neural networks such as AlexNet, LeNet and Inception3, etc. For example, at final epoch (a long training time), the spectra of weight matrices in LeNet+MNIST is MP Law but Heavy Tail in MiniAlexNet+CIFAR10. They observe modern networks on modern data sets seem to achieve Heavy Tail more often, and get a few observations point to the influence of the batch size and training epochs used in the training, but small neural networks could still emerge Heavy Tail. What are the determining factors of these spectral shapes? Very few in the literature have addressed these questions. Recently, [Gurbuzbalaban et al. \(2021\)](#) pointed out that SGD can bring out heavy tails, which partly explained the Heavy Tail spectra. However, the general questions above remain unanswered.

## 2 Data-driven regularization: findings and results

A generally accepted definition of the concept of *Regularization* in a DNN refers to the genesis of certain structure in its weight matrices during the training process. The DNN is well regularized if one is indeed able to identify such specific structures. In this paper, we follow [Martin and Mahoney \(2021\)](#) for considering types of spectra of the weight matrices as an indicator of regularization in the DNNs. Precisely, three types of characteristic spectra are considered in our approach: (i) MP spectrum; (ii) MP spectrum with few bleeding out outliers (MPB); and (iii) HT type spectrum. The transition from MP spectrum, to MPB and HT spectra corresponds to increasingly higher degrees of regularization in the DNN. This correspondence is sketched in Figure 1.

We argue that the achieved regularization in a trained DNN is *data driven*, in the sense that the evolution of regularization depends on the *quality of the data* fed to a DNN. To define this data quality concept, let us consider DNNs that are designed for a classification task. We say that the data has a high quality if the underlying feature classes are well-separated. In this case, the spectra of weight matrices at the final epoch always have the form of a MP Law with few bleeding out outliers (MPB type), or of a sole MP Law (MP type); the DNN shows a low degree of regularization. In contrast, we say that the data has a low quality when the trained feature classes are mixed-up and not well separated; we show that in this situation, the spectra of weight matrices at the final

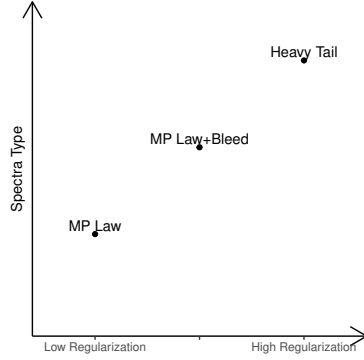


**Figure 1** Correspondence between the degree of regularization in DNN and the spectrum type of its weight matrices.

epoch are always Heavy Tailed (HT type) which indicate a high degree of regularization in the DNN.

In order to give support to this concept of data-driven regularization, this paper proposes three sets of results, summarized in the following three Sections 2.1, 2.2 and 2.3, respectively.

## 2.1 Evidence for Data-Driven Regularization in a Gaussian model

Most deep neural networks are applied to real world data. These networks are however too complex in general for developing a rigorous theoretical analysis. For a theoretical investigation, a widely used and simplified neural network (NN) is the Gaussian input model (Lee et al., 2018).

By examining a well-defined Gaussian model for classification, we establish the evidence for a data-driven regularization via the confirmation of a transition phenomenon in the spectra of network’s weight matrices in the order of MP  $\rightarrow$  MPB  $\rightarrow$  HT. Moreover, the transition is fully controlled by a single parameter of data quality in the Gaussian model, namely its signal-to-noise ratio (SNR).

**Empirically Results:** Signal-to-noise ratio (SNR) is a common indicator to measure data quality and greatly impacts the data structure from a Gaussian model. We empirically examine the spectra by tuning SNR in different architectures:

1. Different NN structures: wider but shallower, or narrower but deeper. These structures are similar to the various well known NNs’ fully connected denser layers, such as LeNet and MiniAlexNet, etc.;
2. Different layers in neural networks: all weight matrices in different layers have spectrum transition driven by SNR;

3. Different class numbers in input data: the spectrum transition is always observed in different class numbers, and the number of spikes is highly related with the number of classes.

Table 1 gives a short summary of the findings.

**Table 1** Summary of spectrum transition in a controlled Gaussian model with  $K$  classes and various SNRs.

SNR	Type of spectra	Number of spikes
Weak	Heavy Tail	$K - 1$ or $K$
Middle	Heavy Tail ↓ MP+Bleed out	$K - 1$ or $K$
Strong	Light Tail (MP Law)	$K - 1$ or $K$

We empirically observe the spectrum transition in all settings. The transition is fully driven by the data SNR. Therefore, in this Gaussian model, the regularization in the trained DNN is data-driven, directly determined by the data SNR. Precisely, under low level SNR, the weight matrices of a DNN deviates far away from the common MP model. Instead, they are connected to very different Heavy Tailed Random Matrix models. The increase of the SNR drives the weight matrices from Heavy Tailed model into MP models at the final training epoch.

Full details on the design of the Gaussian model and the extensive experimental results are reported in Section 3.

## 2.2 Evidence for Data-Driven Regularization in LeNet and MiniAlexNet

The previous results on a Gaussian model are based on synthetic data. Here we conduct experiments with real data sets to show the existence of data-driven regularization. The DNNs chosen for these experiments are the LeNet and MiniAlexNet (LeCun et al., 1998; Krizhevsky et al., 2012), two of the most classic and representative DNNs in pattern recognition. We consider two data sets, the MNIST and CIFAR10. Note that in Martin and Mahoney’s work, the data sets such as CIFAR10, CIFAR100 and Image1000 all bring in HT type spectra unlike the MNIST data set. In our experiments, we select MiniAlexNet instead of the more extensive AlexNet to reduce computing complexity.

Table 2 gives the type of spectra obtained in the trained NNs with each data set.

In training with MNIST, the spectra of weight matrices is always of MP type, independently of the used NN; while for CIFAR10, the spectra are always of HT type for both networks. These experiments show that the degree of regularization achieved in the trained NN is only function of the data sets used (CIFAR10 or MNIST), independently

**Table 2** Spectra types obtained in the four combinations (Data Set) $\times$ NN. Numbers in parentheses are the corresponding detection rates on test data.

Data Set \ NN	LeNet	MiniAlexNet
MNIST	MP (99%)	MP (99%)
CIFAR10	HT (64%)	HT (76%)

of the architecture of the NN (LeNet or MiniAlexNet). This gives new evidence that network regularization is driven by the data.

Moreover, the testing accuracies of detection on MNIST are 99% in both LeNet and MiniAlexNet, while those on CIFAR10 are 64% with LeNet, and 76% with MiniAlexNet, respectively. These indicate that MNIST and CIFAR10 have very different data structures and data qualities. The higher quality of MNIST brings in the MP Law type in the final spectra of weight matrices, indicating a low regularization in the trained networks. On the contrary, lower quality of CIFAR10 brings in the Heavy Tail shape for weight matrix spectra, indicating a high degree of regularization in the trained NNs.

Full details for these experimental results are reported in Section 4.

### 2.3 A spectral criterion for early stopping

As a regularization technology in Deep Learning, early stopping is adopted to improve generalization accuracy of a DNN. People may use testing data set to obtain convenient stopping time in practice, but when we model the data set, it is a trade off to separate data set into training and testing, and sometimes, it is more expensive to acquire the testing data set (Martin et al., 2021). There are also situations where practitioners of Deep Learning are laid to use pretrained and existing DNNs without access to test data.

So an important question we address here is: Without any testing data set, shall we early stop or not? And how to define an early stopping time?

Because we could characterize the degree of achieved regularization during a training process by its correspondence with the spectrum type of weight matrices, we construct an application of the phenomenon to guide the early stopping of the training through a **Spectral Criterion**. Precisely, we introduce a distance between an observed weight matrix spectrum and the reference MP Law. When this distance is judged large enough, we obtain evidence for the formation of a HT type spectrum, thus a high regularization of the DNN which leads to the decision of stopping the training process. Note that this spectral criterion for early stopping does not need any test data.

We now describe this spectral criterion in more details. Consider a  $n \times N$  ( $n \leq N$ ) weight matrix  $W$  and let  $X_1, X_2, \dots, X_n$  be the  $n$  non-zero eigenvalues of the square matrix  $WW^T$ . (These are also, by definition, the squares of the singular values of the

matrix  $W$ . The initialization of  $W$  has been rescaled with  $1/\sqrt{N}$ .) We then construct a histogram estimator  $\hat{p}_M(x)$  for the joint density of the eigenvalues using  $M$  bins. Next, let  $p_{c,\sigma^2}(x)$  be the reference Marčenko-Pasture density (Appendix B) depending on a scale parameter  $\sigma^2$  and a shape parameter  $0 < c < 1$ , with a compact support  $[a, b]$  ( $0 < a < b$ ). In practice, the parameters  $c$  and  $\sigma^2$  in the reference MP density  $p_{c,\sigma^2}(x)$  are also estimated by using  $X_1, \dots, X_n$ . This leads to an estimated MP density function  $p_{\hat{c},\hat{\sigma}^2}(x)$ . The estimation of distance between the distribution of the  $n$  eigenvalues and the MP density is defined as  $L_1$  distance

$$\hat{s}_n = \int_a^b |\hat{p}_M(x) - p_{\hat{c},\hat{\sigma}^2}(x)| dx. \quad (1)$$

Under the null hypothesis that the eigenvalues  $\{X_i\}$  follow the MP law, we have a precise rate for  $\hat{s}_n \rightarrow 0$ , which leads to our spectral criterion.

**Spectral criterion.** Set  $M = 2\lceil n^{\frac{1}{3}} \rceil$  and consider a threshold value  $s_* = C * \sqrt{\log n}/n^{\frac{1}{3}}$  with  $C = 0.4$ . For each training epoch, calculate  $\hat{s}_n$  in equation (1) by the **Algorithm** in Appendix D. The training is stopped if  $\hat{s}_n > s_*$ .

(To gain more robustness in this stopping procedure, in all the experiments, we will stop the training at three consecutive epochs where  $\hat{s}_n > s_*$  happen (instead of at the first such epoch).)

The whole details on the determination of the distance value  $\hat{s}_n$  and the threshold value  $s_*$  are given later in Section 5.1. One may ask **why the appearance of a HT spectrum is a good early stopping time?** Let us elaborate more on the important reasons for the early stopping rule above based on the appearance of a HT spectrum. (Martin et al., 2021) mentioned that MP Law spectra could not evaluate the performance of the trained model, but Heavy Tail spectra could. The Heavy Tail spectra may correspond to better or worse test performance. From a data-driven regularization perspective, we bring new insights to such observation. We argue that the regularized structure in the weight matrix is driven by data quality, and as the hyperparameters of a DNN are getting fixed, the emergence of Heavy Tail or Rank Collapse in weight matrices could be viewed in two ways:

- Indication of the poor quality in the training data or the poor ability in the whole system: in numeric experiments, HT always appears when SNR is low. Such poor training data or system quality will lead to instability or overfitting during the whole training dynamics. So the emergence of Heavy Tail can be treated as an **alarm** for these hidden and problematic issues in the network.
- Indication of a regularized structure that has acquired considerable information from the training data: from another point of view, the HT phenomenon is far from the initial MP Laws introduced with random weight initialization. Its emergence

can be viewed as an indication of a well-trained structure that has already captured sufficient information from the input data. Such structure will somehow ensure the testing accuracy of the whole system, and additional training will not bring much improvement.

The spectra criterion is validated in both numeric and real data experiments. Evidence for this **spectral criterion** is developed in details with extensive experimental results in Sections 3.3 and 4.3. In numeric experiments, the spectral criterion provides an early stopping epoch where the testing accuracy is much higher than the final testing accuracy, even when the training accuracy is still increasing. In real data experiments, the spectral criterion could also offer high-quality stopping time, ensuring testing accuracy and cutting off a large unnecessary training time.

### 3 Analysis of a Gaussian model and experimental results

#### 3.1 Gaussian model and Data Sets

In the multi-classification task, Gaussian model is a commonly used model for assessing theoretical properties of a learning system (Lee et al., 2018). In this model with  $K$  classes, data from a class  $k \in \{1, \dots, K\}$  are  $p$ -dimensional vector of the form

$$h_{i,k} = \mu_k + \varepsilon_{i,k}, \quad 1 \leq i \leq n_k, \quad (2)$$

where  $\mu_k \in \mathbb{R}^p$  is the class mean,  $\varepsilon_{i,k} \stackrel{iid}{\sim} \mathcal{N}(0, \sigma^2 I_p)$  are Gaussian noise,  $n_k$  is the total number of observation from class  $k$ . (This Gaussian data model is referred to as the  $K$ -way ANOVA model in the statistics literature.)

The signal-to-noise ratio (SNR) for this  $K$ -class Gaussian model is defined as

$$\text{SNR} = \text{Ave}_{\{k,k'\}} \frac{\|\mu_k - \mu_{k'}\|}{\sigma}. \quad (3)$$

Here  $\|\cdot\|$  denotes the Euclidean norm in  $\mathbb{R}^p$ , and the average is taken over the  $\binom{K}{2}$  pairs of classes.

We aim to examine the impact of the model SNR on the regularization produced in a trained NN for such Gaussian data. We thus consider two settings for the class means  $\{\mu_k\}$  which lead to different families of SNRs.

In all the remaining discussions, we will take  $\sigma = 1$ .

### Model $\mathcal{D}_1(\delta)$ : class means with randomly shuffled locations

Consider a base mean vector  $u = (m, \dots, m, m + \delta, \dots, m + \delta)^T \in \mathbb{R}^p$  where half of the components are  $m$ , and the other half,  $m + \delta$ . For the class means  $\mu_k$ , we reshuffle the locations of these components randomly (and independently). Formally, for each class  $k$ , we pick a random subset  $I_k \subset \{1, \dots, p\}$ , of size  $p/2$ , and define the mean for this class as

$$\mu_k = m\mathbf{1}_{I_k} + (m + \delta)\mathbf{1}_{I_k^c}. \quad (4)$$

Here for a subset  $A \subset \{1, \dots, p\}$ ,  $\mathbf{1}_A$  is the indicator vector of  $A$  with coordinates  $\mathbf{1}_A(i) = \mathbf{1}_{\{i \in A\}}$  ( $1 \leq i \leq p$ ).

This setting with randomized locations is motivated by an essential empirical finding from exploring a few classical trained DNNs such as MiniAlexNet and LeNet. Indeed, we found that in these DNNs, the global histograms of the features from all the neurons are pretty similar, with very comparable means and variances, for various NNs; the differences across the NNs are that high and low values of the features appear in different neurons (locations). The randomly shuffled means used in our experiments are designed to imitate these working mechanisms observed in real-world NNs.

It follows that for the difference  $\mu_k - \mu_{k'} = (z_j)$ ,  $1 \leq j \leq p$  from two classes  $k \neq k'$ , its coordinates  $z_j$  take on the values  $-\delta$ ,  $0$  and  $\delta$  with probability  $\frac{1}{4}$ ,  $\frac{1}{2}$  and  $\frac{1}{4}$ , respectively. Clearly, the model SNR will depend on the tuning parameter  $\delta$ . By Hoeffding inequality, we first conclude that

$$P\left(\left|\frac{\|\mu_k - \mu_{k'}\|^2}{p} - \frac{\delta^2}{2}\right| \leq \epsilon\delta^2\right) \geq 1 - \exp(-2\epsilon^2 p),$$

or equivalently,

$$P\left(\frac{\delta}{\sqrt{2}}\sqrt{1-2\epsilon} \leq \frac{\|\mu_k - \mu_{k'}\|}{\sqrt{p}} \leq \frac{\delta}{\sqrt{2}}\sqrt{1+2\epsilon}\right) \geq 1 - \exp(-2\epsilon^2 p)$$

Note that  $\sqrt{1+x} \leq 1+x$ ,  $\sqrt{1-x} \geq 1-x$  when  $0 < x < 1$ . By taking  $\epsilon = \sqrt{\log p/p}$ , we conclude that with probability at least  $1 - 1/p^2$ ,

$$\left|\|\mu_k - \mu_{k'}\| - \delta\sqrt{\frac{p}{2}}\right| \leq \delta\sqrt{2\log p}.$$

Therefore at a first-order approximation, the SNR (3) in this Gaussian model is (with  $\sigma = 1$ ),

$$\text{SNR} = \text{Ave}_{\{k, k'\}} \frac{\|\mu_k - \mu_{k'}\|}{\sigma} \sim \delta\sqrt{\frac{p}{2}}. \quad \square \quad (5)$$

### Model $\mathcal{D}_2(t)$ : class means of ETF type

Consider the family of vectors  $\{v_k\}_{1 \leq k \leq K}$  where  $v_k$  is defined by

$$v_k = \mathbf{1}_{\{i=k\}} - \frac{1}{K} \mathbf{1}_{\{1 \leq i \leq K\}}, \quad 1 \leq i \leq p.$$

So  $v_k$  has support on  $\{1, \dots, K\}$  and  $\|v_k\| = \sqrt{(K-1)/K}$ . The normalized family  $\{v_k/\|v_k\|\}$  is called a  $K$ -standard ETF structure (Pappyan et al., 2020).

We define the  $k$ -th class mean as  $\mu_k = tv_k$ , and use the scale parameter  $t > 0$  to tune the SNR of the model. It is easy to see that  $\|\mu_k - \mu_{k'}\| = \sqrt{2}t$  so that the model SNR is

$$\text{SNR} = \underset{\{k, k'\}}{\text{Ave}} \frac{\|\mu_k - \mu_{k'}\|}{\sigma} = \|\mu_k - \mu_{k'}\| = \sqrt{2}t. \quad (6)$$

(Pappyan et al., 2020) has shown that the ETF structure is an optimal position for the final training outputs. Many experiments on real data sets lead to ETF structure for final engineered features. From a layer-peered perspective as mentioned in (Ji et al., 2021), each layer in NN can be regarded as an essential part of feature engineering, and the feature is extracted layer by layer. The ETF structure model considers that the first Dense layer behind the convolution layer is already close to the end of feature extraction.

In our experiments, we take  $m = -0.2$  (and  $\sigma = 1$ ). The size of each class  $k$  is  $n_k = 7500$  in the training dataset, and  $n_k = 800$  in test dataset. The number of classes  $K$  takes on the values  $\{2, 5, 8\}$  on all datasets. Table 3 gives the ranges of the model SNR observed in different dataset/NN combinations with the chosen values of tuning parameters  $\delta$  and  $t$ .

**Table 3** Ranges of SNRs observed in various datasets/ networks combinations.

	$\mathcal{D}_1(\delta)$		$\mathcal{D}_2(t)$	
	$\delta$	SNR interval	$t$	SNR interval
NN1	0.01	[0.01, 1.19]	0.08	[0.08, 4.80]
	0.05	[1.20, 2.00]		
NN2	0.005	[0.005, 0.4]	0.08	[0.08, 4.80]

#### 3.1.1 Structure of neural networks

We consider two different neural networks, a wider but shallower NN1, and a narrower but deeper NN2. The number of layers and their dimensions are shown in Figure 2:

$$\text{NN1: } 100 \rightarrow 1024 \rightarrow 512 \rightarrow 384 \rightarrow 192 \rightarrow K,$$

NN2:  $2048 \rightarrow 1024 \rightarrow 512 \rightarrow K$ .

The activation function is  $\text{ReLU}(x) = \max(x, 0)$ . We do not apply any activation function on the last layer.

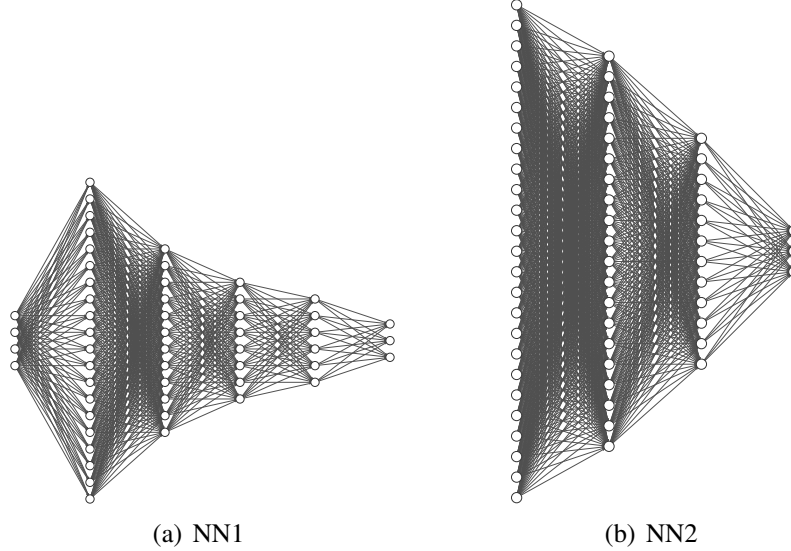


**Figure 2** The two NNs considered which imitate the dense layer in well-known NNs such as MiniAlexNet, VGG and LeNet.

### 3.1.2 Optimization Methodology

Following common practice, we minimize the cross-entropy loss using stochastic gradient descent with momentum 0.9. All the datasets are trained with batch size =64 on a single GPU, for 248 epochs. Trained NNs are saved for the first 10, and then every four epochs. The total number of saved NNs is  $(136+60+80+60) \times 3 \times 70 = 70560$ . The initialization is Pytorch’s default initialization, which follows a uniform distribution. The learning rate is 0.01.

## 3.2 Results on Data-Driven Regularization

To investigate the influence of the data SNR on the whole training process, we first report numeric experiments results.

### 3.2.1 Spikes away from spectrum bulk

There is always a visible gap between spectrum bulks and spikes away from them. A few examples are given in Figure 3 that come from the second layers’ eigenvalues at

final epoch in the four different experiments (with specific tuning parameter).

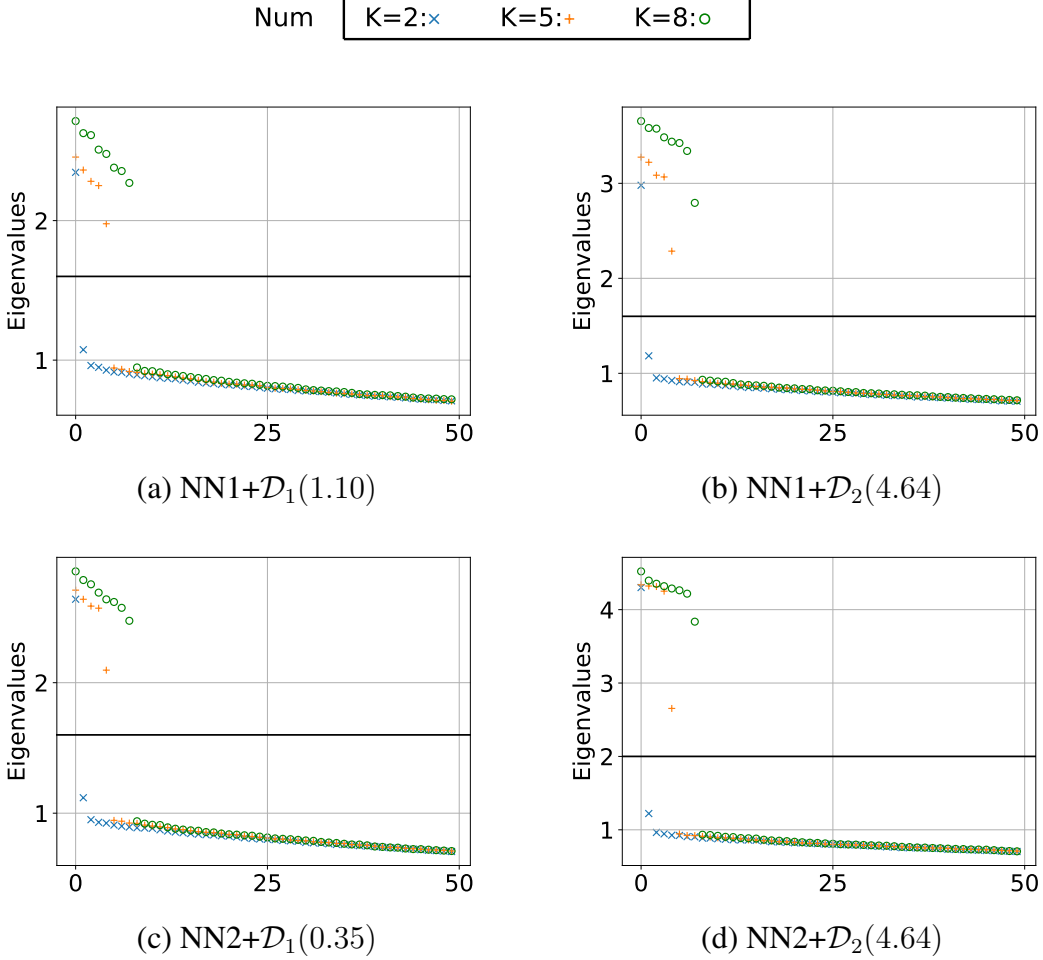


**Figure 3** Spikes and Spectrum Bulk: The solid line represents visible gaps between spikes and spectrum bulk in the experiments. Eigenvalues are sorted in descending order.

**Number of spikes and their separation:** When the NN is getting more and more regularized, the spectra of weight matrices which show a large base bulk and a number of spikes that lay away from the bulk. The appearance of such spike eigenvalues is also reported for other matrices in NNs, such as Loss Hessian matrix and layers’ feature out covariance matrix (Sagun et al., 2017; Pappan, 2019b; Martin and Mahoney, 2021).

We empirically observed the *separation* of spikes: they are grouped in (i) a distant block of  $K - 1$  values, and (ii) a single spike between this block and the spectrum bulk. This separation phenomenon is particularly visible in the Figures 3-(b) and (c).

However it remains unknown how training dynamics create these spikes, and how the class number affect the number of spikes in such deep neural networks under SGD.

But our experiments show that the number of observed spikes is highly connected to the number of classes in the input data.

### 3.2.2 Three types of spectrum bulk

We use SNR to measure the data quality and focus on the non-zero eigenvalues of the matrix  $WW^T$ . The weight matrices  $W$  we consider in this section are those at the final epoch (248th). In the Gaussian model, with different values of SNR, we have observed the following three typical types for the bulk spectrum of the weight matrices:

**HT** : Heavy Tail

**MPB** : MP Law (Bleed Out)

**MP** : MP Law (Light Tail)

We use "XX(m,n)" to describe the whole ESD type of the spectrum of weight matrices. Here "XX" means one of the three bulk types in {HT, MPB, MP}. The number "m" means the number of spikes which lay between the spectrum bulk and the block of distant spikes, "n" means the number of distant spikes. For instance, MPB(1,7) displayed in Figure 5(d), means the bulk type is "MP Law (Bleed out), 1 between spike and 7 distant spikes". We give more details on the spectra type classification as shown in Figures 4-7. In all figures, a solid curve shows the MP density that fits the observed spectrum bulk best. A poor fit reflects the existence of a HT type or MPB type spectrum bulk.

**Heavy Tail:** Low SNR in the training data leads to the Heavy Tail phenomenon. The shape of ESD of weight matrices deviates from MP Law and is similar to the Power fit Law. The four pictures in Figure 4 are all possible to appear during the training process. The separation of spikes away from the bulk matches the block  $K - 1$  and the single "one", and the shape is no longer MP like, which indicates large training information.

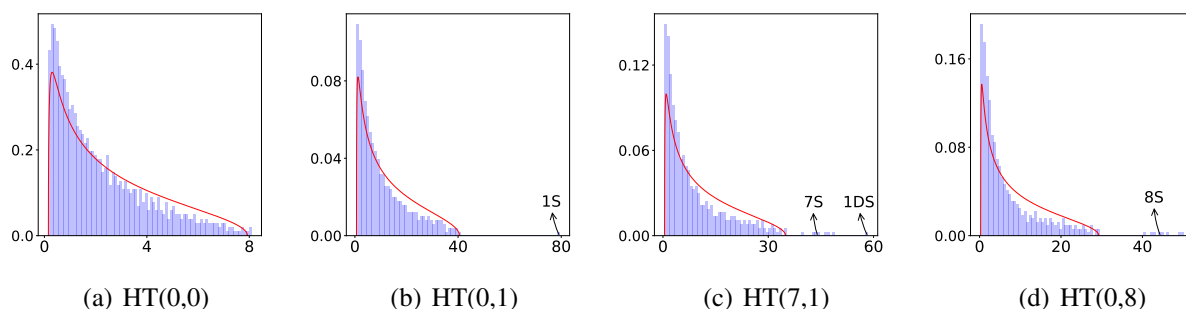


**Figure 4** Examples of observed Heavy Tail type spectrum bulks.

**MP Law(Bleed Out):** In the case MPB emerges, SNR is larger than the case where Heavy Tail emerges, and smaller than the case where the spectrum bulk is MP Law like. As shown in Figure 5, MPB is in the middle transition from HT to MP, Figure 5(a) or 5(b)  $\rightarrow$  Figure 5(c) or 5(d)  $\rightarrow$  Figure 6, with increment of SNR. We detect the bulk transition (BT) period when the block  $K - 1$  eigenvalues become distant.

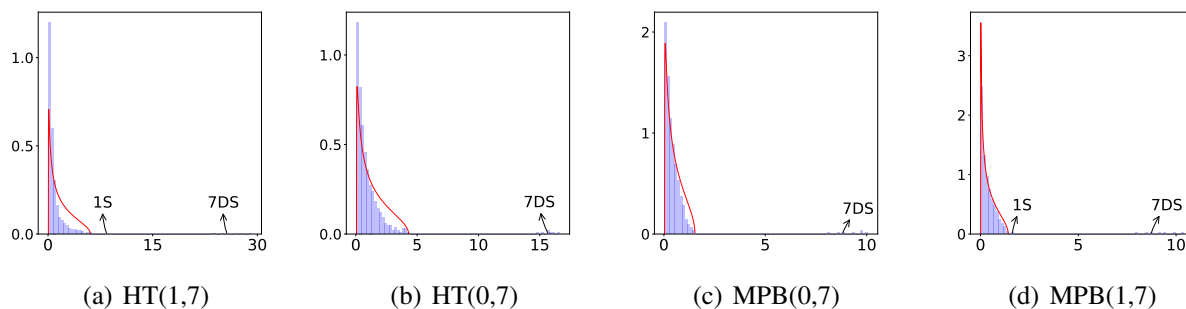


**Figure 5** Examples of observed MPB type spectrum bulks.

**Light Tail:** We detect the Light Tail period when the spectrum bulk well fits a MP Law. The spikes still consist of between and distant eigenvalues. When SNR is large, Light Tail Phenomenon always exists, and the shape is MP Law as shown in Figure 6.

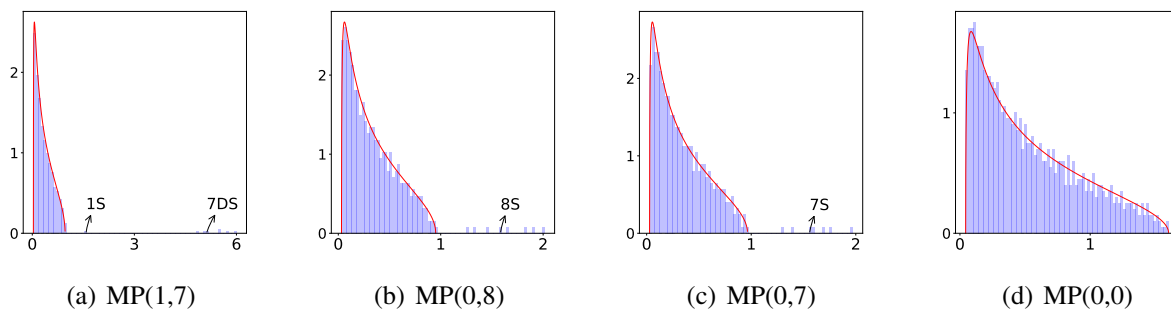


**Figure 6** Examples of observed MP type spectrum bulks.

**Rank Collapse:** One special case, Rank Collapse, occasionally emerges in our experiments especially when SNR is small. Rank Collapse is the phenomenon that the spike is huge, making the bulk in the picture 'needle like' as shown in Figure 7. By tuning up SNR, Rank collapse gradually disappears and turns into Light Tail or Heavy Tail.

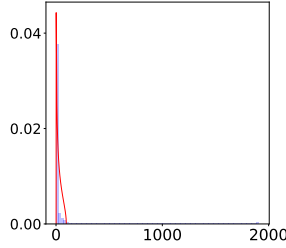


**Figure 7** Example of spectrum with Rank Collapse.

### 3.2.3 Phase Transition

We now describe evidence that the spectrum bulks of weight matrices undergo a phase transition controlled by the data SNR. The phase transition operates in the direction of

$$\text{HT} \rightarrow \text{MPB} \rightarrow \text{MP}$$

when the SNR increases. The complete experimental results, with recorded phase transition periods (in terms of intervals of SNR values) in all NN layers, are given in Table 6-9 in Appendix A, for the four NNs/datasets combinations respectively. These tables are summarized in Figure 8 as a graphical summary.

The main findings from these results are as follows:

- (1) When the SNR increases, all spectrum bulks in weight matrices fall into the MP type at final epoch. The four subfigures for the NNs/datasets combinations all contain the **Same Transition Period Direction**:

$$\text{Heavy Tail} \rightarrow \text{Bulk Transition} \rightarrow \text{Light Tail.}$$

In our experiments, the bulk transition (BT) period starts when the block  $K - 1$  eigenvalues become distant, and the Heavy Tailed spectrum bulk gradually changes into MPB type with an increment of SNR. It is also noted that some weight matrices start from MPB type and MP type, then transit in the same direction. The same transition direction provides us SNR-driven regularization in this Gaussian model.

- (2) One interesting phenomenon is that when one travels from the initial layer to deeper layers (FC2→FC4 in NN1, FC1→FC2 in NN2), the tails of spectrum bulks become lighter. This is true for both NNs and all SNR levels. Recall that SNR is the quality measurement of the feature output in the initial layer, and lighter tails mean higher SNRs; we can interpret this phenomenon as the fact that the data quality (SNR) of the feature indeed increase from initial layers to deeper layers. This conclusion is quite expected. Pappayan et al. discovered the optimal structure ETF for the last layer’s output in various neural networks, which also supports the feature extraction in DNNs. The

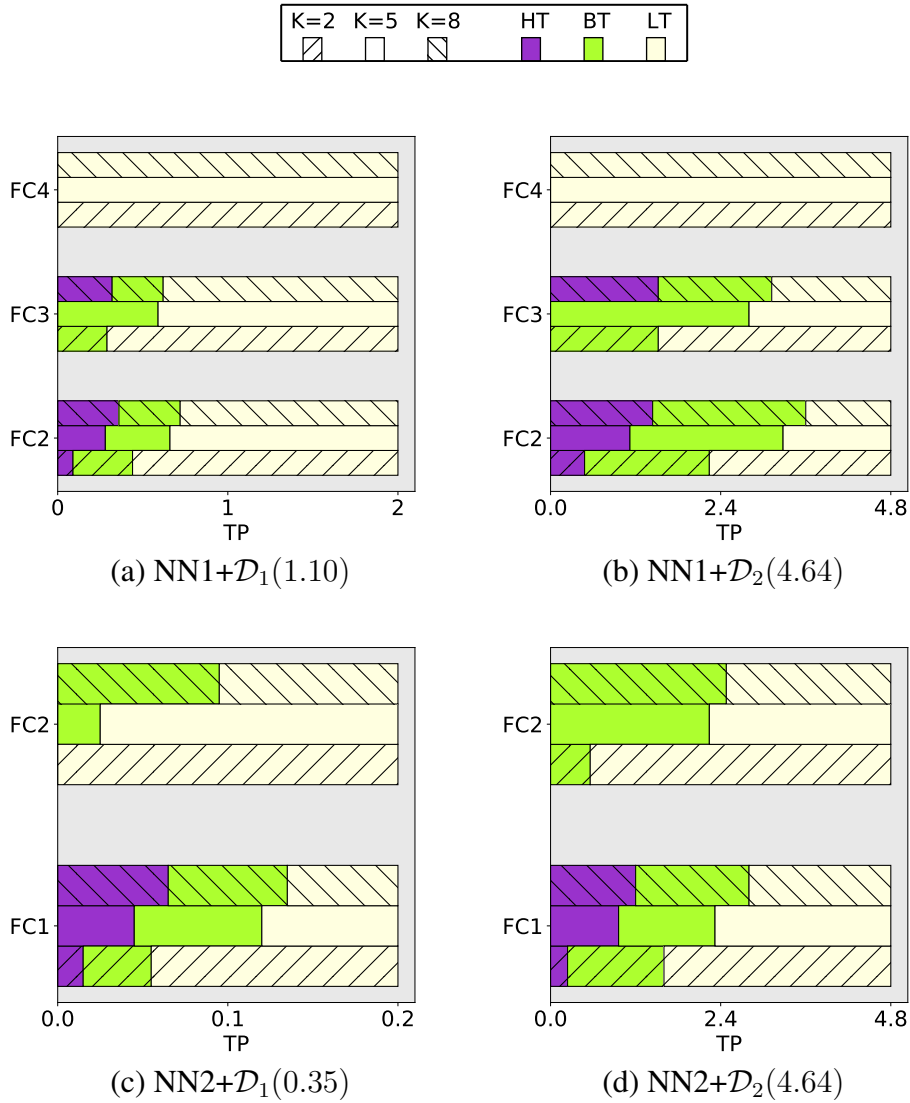


**Figure 8** Transition Period with the four NNs/datasets combinations. The x-axis is the tuning parameter (TP) to tune the SNR level with the range given in Table 3. Each block of three lines in a given layer corresponds to the cases  $K = 8$  (Topline),  $K = 5$  (Middle line) and  $K = 2$  (Bottom line). Different colors represent different transition periods

interesting aspect in our paper is that we can confirm it by observing the type of their respective spectra. Unlike the previous layers, the last layer in DNNs is the decoder part which achieves ETF structure to decode the extracted features.

(3) For a given layer in the neural network at the same SNR level, the tails of spectrum bulks become heavier as the number of classes  $K$  increases. When the SNR level is the same, the more classes the data set has, the more regularization structures in neural networks are required to classify each category. The phenomenon that spectrum bulks become heavier with an increased number of classes  $K$  also gives direct evidence of data-driven regularization.

Indeed, the HT type spectra correspond to higher regularization being formed in the NNs; by contrast, a MB type bulk spectrum reflects a lower degree of regularization. Heavy Tail phenomena always lie in the low SNR period, which means that the training on low SNR or poor quality data set brings a higher regularization in the NNs to detect the features in the data, which also gives us alarm on the hidden and problematic issues as Section 2.3 mentioned if HT emerges. In other words, the data quality, which is characterized by the SNR in the Gaussian model, directly impacts the degree of regularization produced by the training process in the NNs, thus brings new insights into Deep Learning.

### 3.2.4 Additional experiments on different batch sizes

Batch size also has great impact on the training stability together with data features. (Keskar et al., 2016; Goyal et al., 2017) observe that different batch sizes may give different influence on the training dynamics. Does Data-Driven Regularization exist on different batch sizes? Does the number of spikes match the class number well under different batch sizes? The answer is yes. To give more comprehensive evidence of Data Driven regularization, we change data features on different batch sizes, and conduct experiments on  $\text{NN1}+\mathcal{D}_1$  and  $\text{NN2}+\mathcal{D}_2$  with  $K = 8$ , and two additional batch sizes 256, 32 (previous experiments all used a batch size of 64).

The number of spikes still equals to  $K$  or  $K - 1$  and the separation of spikes still exist under various settings, as shown in Figure 9. We further check the transition. The phase transition of the spectrum bulk is still observed in the same direction as previously (HT→Bulk Transition→LT). Full results are given in Table 10-11 in Appendix A. Again, a summarized visualization is given in Figure 10. The settings are all similar to those used previously.

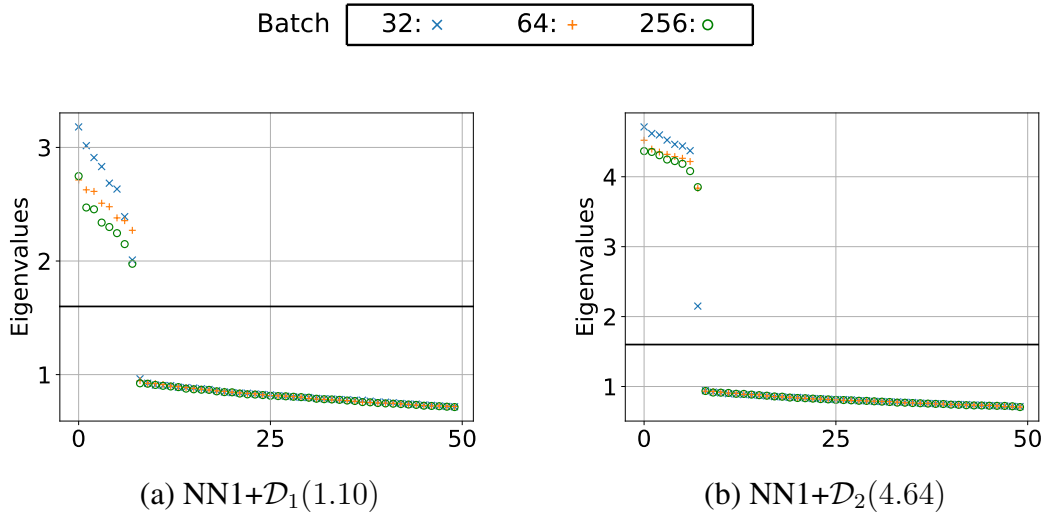


**Figure 9** The visible gaps in the extra experiments, set different batch sizes.  $x$ -axis is the order of eigenvalues,  $y$ -axis is the corresponding value of eigenvalues. Both figures are obtained in the FC2 layer.

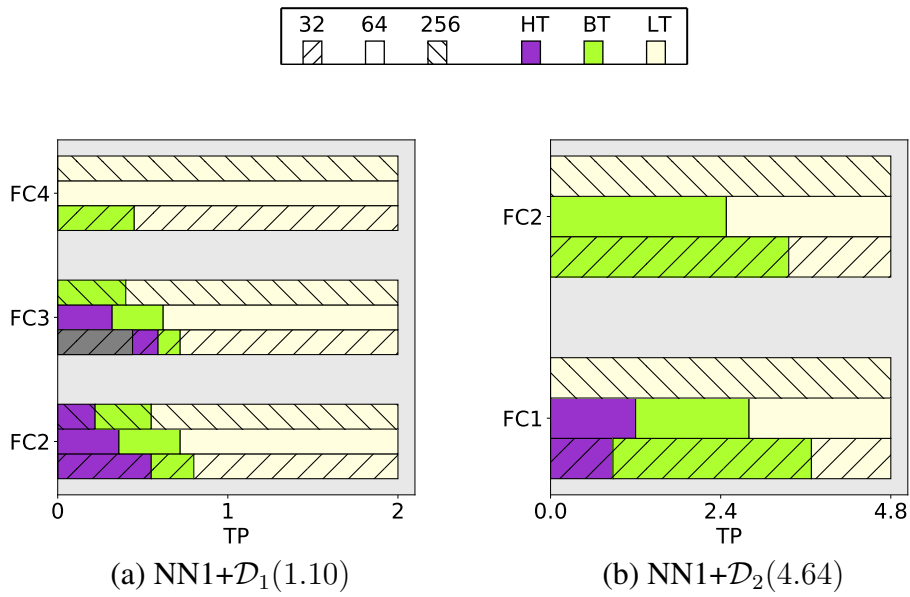


**Figure 10** Transition Period in different batch sizes. The gray part in  $\text{NN1}+\mathcal{D}_1$  at FC3 represents Rank Collapse.

### 3.3 Early stopping with the spectral criterion

Because of huge amount of data under analysis, we conduct experiments, stock the relevant data, and then check the results offline. The epochs where we save trained NNs for different architectures are all fixed at 0, 1, 2,..., 9, 10, 12, 16, 20,..., 248, the latter epochs having an increment of four. Even in such sparse data reservation, the total data we obtained is larger than 1TB.

We apply the spectra criterion developed in Section 2.3 to the stocked training epochs, and decide the early stopping time if the criterion is met. When this happens, we compare the test accuracy of the corresponding NN with that of the NN trained till the final epoch (248th). This comparison serves to measure the quality of the early stopping using the spectral criterion. Experiment results with  $K = 8$  are shown in Table 4 and Figure 11.

#### Comments:

- $\text{NN1}+\mathcal{D}_1$  and  $\text{NN1}+\mathcal{D}_2$ : During the first 20 epochs when SNR is low, the testing accuracy is decreasing while the training accuracy is increasing. Spectral criterion detects such hidden and problematic issues and recommends to early stop. It is truly remarkable that almost all early stopped NNs have higher test accuracies than the corresponding NNs trained till the end. The advantage is particularly important when the SNR is low. When SNR is large, there might be no alarm by the spectral criterion, see the situation of TP=0.9 in  $\text{NN1}+\mathcal{D}_1$  and TP=4.8 in  $\text{NN1}+\mathcal{D}_2$ . This is in fact a consistency of the spectral criterion, no early stopping is needed, and the fully trained NNs have indeed higher test accuracies.
- $\text{NN2}+\mathcal{D}_1$  and  $\text{NN2}+\mathcal{D}_2$ : Spectral Criterion detects stopping time under low SNR, nonetheless the testing accuracy is a little lower than the final testing accuracy. As the differences are very small, huge training time is cut off, and testing accuracy is ensured due to the emergence of well-trained structure that already seized sufficient information.

The spectral criterion is valid when overfitting appears in training. In such situation, the training and testing accuracies do not have the same tendency. As training epochs increase, Figure 11 shows that training accuracy tends to 100% while testing accuracy is highly related with the tuning parameter  $\delta$  or  $t$ . Without testing data, the spectral criterion could propose an early stopping time even when the training accuracy is increasing.

When the spectral criterion gives different epochs in different layers, there is a question that **how to decide a stopping time?** From our experimental results, we empirically suggest that any epoch after the time some layer hits the critical value  $s_*$  is suitable to stop, and it is strongly recommended to stop training if there is more than one layer

**Table 4** Early stopping results in numeric experiments with  $C = 0.4$ : stopping epochs selected by spectral criterion in different layers' weight matrices and their testing accuracy (Test Acc). The symbol "-" means no early stopping epoch is found by the spectral criterion.

The combination NN1+ $\mathcal{D}_1$

Typical TP	spectral criterion $C = 0.4$				Final Epoch 248		
	epoch(FC2)	Test Acc	epoch(FC3)	Test Acc	FC1	FC2	Test Acc
0.15	7	25.84%	10	23.23%	HT	HT	20.17%
0.2	7	32.70%	12	27.48%	HT	HT	27.03%
0.3	7	49.36%	12	45.48%	HT	HT	44.80%
0.6	8	88.52%	32	88.32%	MPB	MPB	88.30%
0.9	-		-		MP	MP	99.13%

The combination NN1+ $\mathcal{D}_2$

Typical TP	spectral criterion $C = 0.4$				Final Epoch 248		
	epoch(FC2)	Test Acc	epoch(FC3)	Test Acc	FC1	FC2	Test Acc
0.24	9	14.69%	16	13.89%	HT	HT	13.08%
1.2	7	38.61%	12	35.84%	HT	HT	32.98%
2.4	7	77.19%	16	74.55%	HT	HT	75.92%
3.2	9	92.11%	-		HT	MPB	92.64%
4.8	-		-		MP	MP	99.73%

The combination NN2+ $\mathcal{D}_1$

Typical TP	spectral criterion $C = 0.4$				Final Epoch 248		
	epoch(FC1)	Test Acc	epoch(FC2)	Test Acc	FC1	FC2	Test Acc
0.02	6	14.89%	7	15.84%	HT	MPB	16.02%
0.04	8	24.78%	7	23.34%	HT	MPB	25.38%
0.07	5	48.31%	6	48.63%	HT	MPB	50.12%
0.13	6	87.03%	-		MPB	MP	87.50%
0.2	-		-		MP	MP	99.14%

The combination NN2+ $\mathcal{D}_2$

Typical TP	spectral criterion $C = 0.4$				Final Epoch 248		
	epoch(FC1)	Test Acc	epoch(FC2)	Test Acc	FC1	FC2	Test Acc
0.24	10	13.08%	6	12.89%	HT	HT	13.44%
1.2	12	34.22%	5	34.63%	HT	HT	36.31%
2.4	5	72.59%	16	74.61%	MPB	MPB	75.12%
3.2	-		-		MP	MP	91.20%
4.8	-		-		MP	MP	99.59%

hitting the critical value. For example,  $TP=0.15$  in  $NN1+\mathcal{D}_1$ , epochs in 7-10 are all suitable early stopping time with a guaranteed test accuracy.

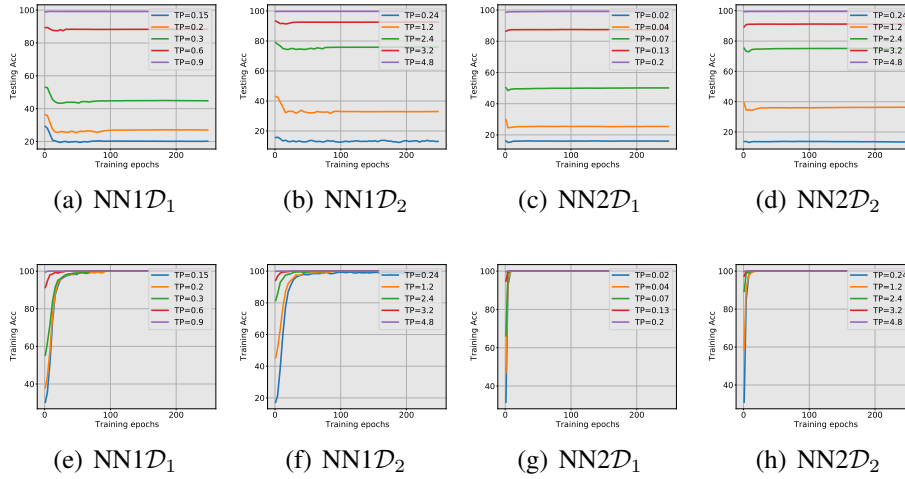


**Figure 11** Testing and Training Accuracy: We begin the line at epoch=1. Testing accuracy: (a)-(d); Training accuracy: (e)-(h). y-axis is the accuracy value, x-axis is the training epochs. Different line represents different SNRs in data sets.

## 4 Analysis and experiments with real data sets

### 4.1 Experimental Design

The structures of LeNet and MiniAlexNet are shown in Figure 12. The data sets we use are MNIST and CIFAR10. We tune batch sizes to have different practical architectures, then check spectra type and **spectral criterion** in the different data sets under such different practical architectures. As before, we save trained models for the first 10 epochs and every four epochs afterward. The optimization methodology is the same as previously (See Section 3.1.2).

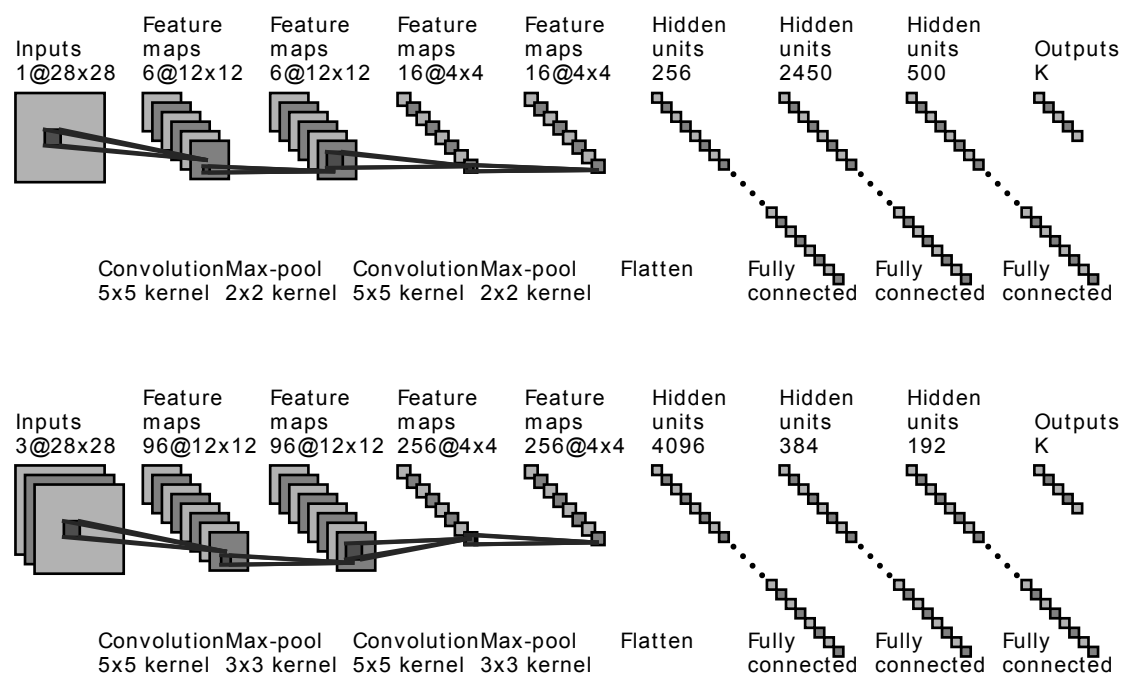


**Figure 12** The structure of LeNet (top) and MiniAlexNet (Bottom). The input data sets are MNIST with size  $1 \times 28 \times 28$  or CIFAR10 with resize  $3 \times 28 \times 28$ , the fully connected layers lay behind convolutional layers.

### 4.2 Results on Data-Driven Regularization

At the final epoch, the ESDs in LeNet and MiniAlexNet essentially reflect the characteristic features of the data in MNIST and CIFAR10. We concentrate on weight matrices in Fully connected layers and display the results in Figure 13-16.

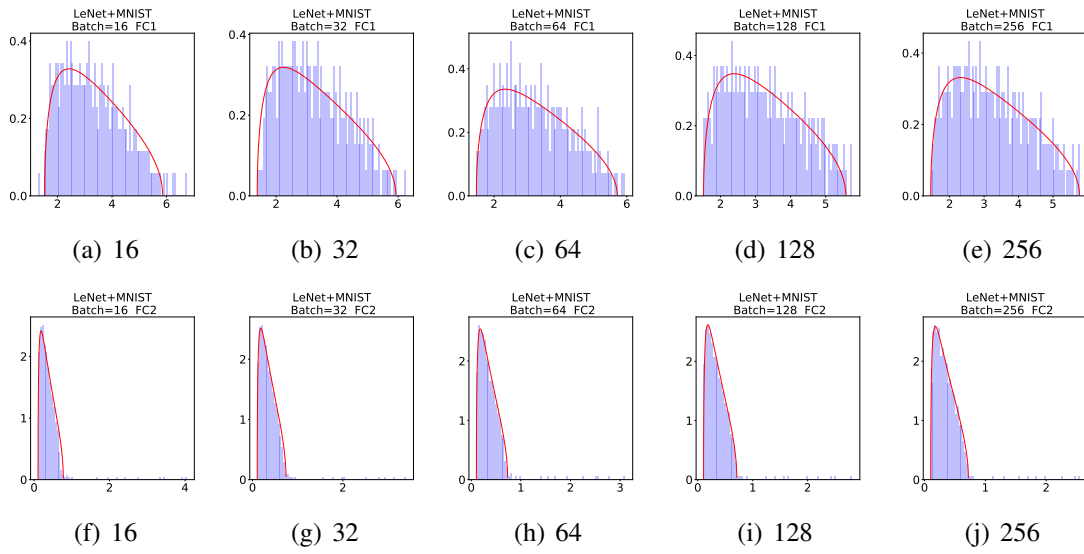


**Figure 13** LeNet+MNIST: Weight matrix spectra at final epoch 248. FC1 layer: (a)-(e); FC2 layer: (f)-(j). Columns show experiments with different batch sizes.

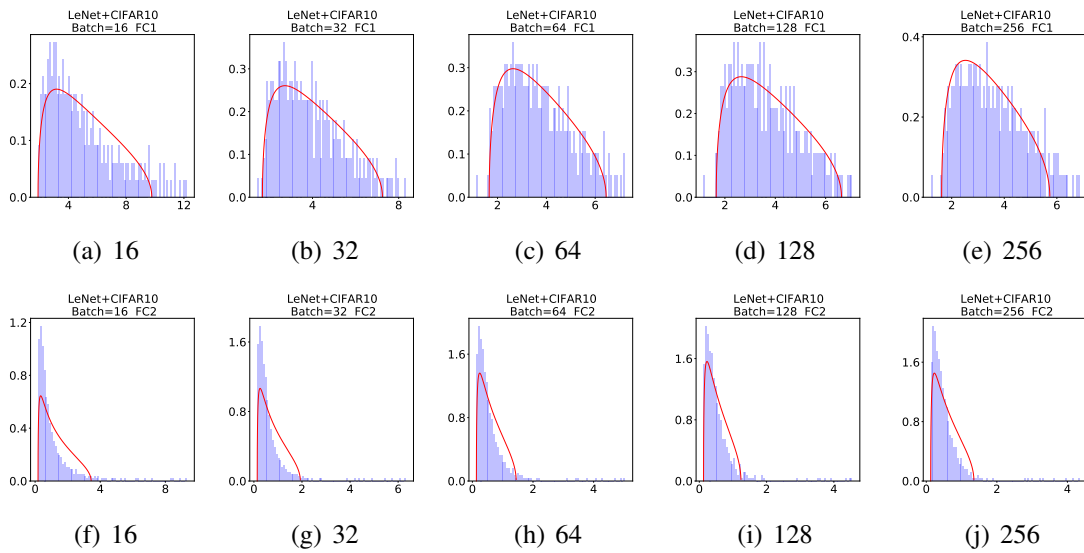


**Figure 14** LeNet+CIFAR: Weight matrix spectra at final epoch 248. FC1 layer: (a)-(e); FC2 layer: (f)-(j). Columns show experiments with different batch sizes.

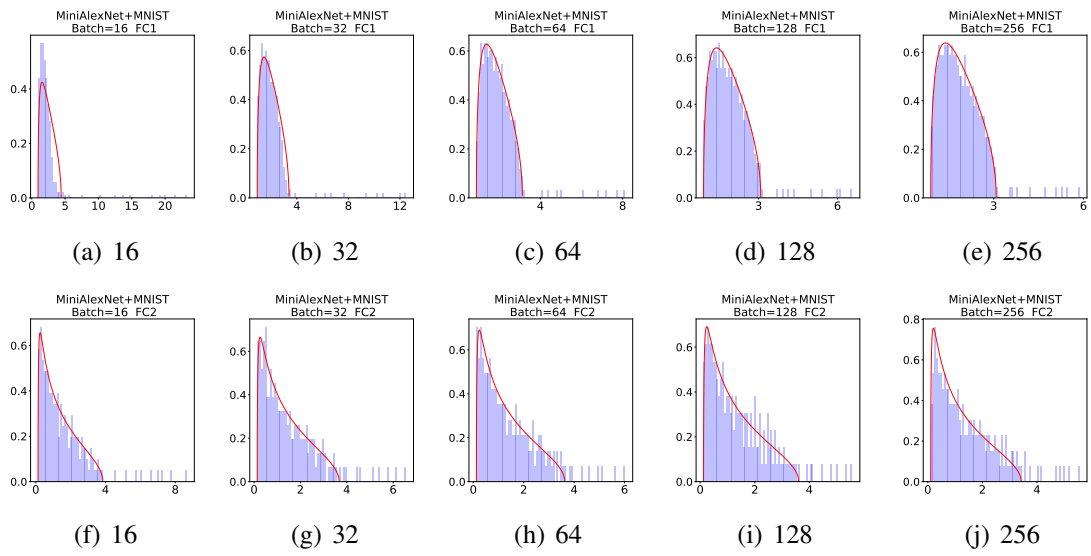


**Figure 15** MiniAlexNet+MNIST: Weight matrix spectra at final epoch 248. FC1 layer: (a)-(e); FC2 layer: (f)-(j). Columns show experiments with different batch sizes.

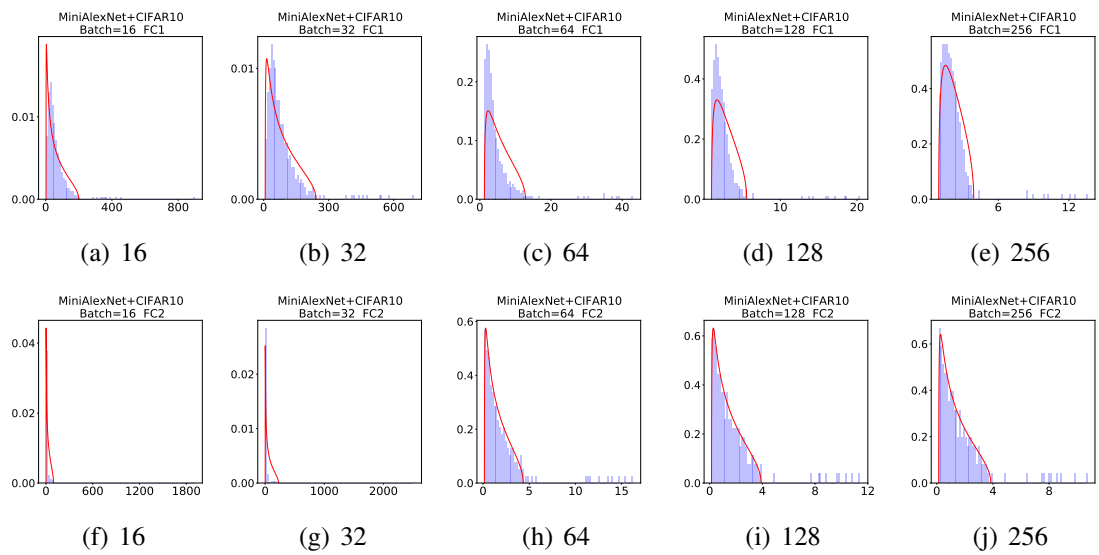


**Figure 16** MiniAlexNet+CIFAR: Weight matrix spectra at final epoch 248. FC1 layer: (a)-(e); FC2 layer: (f)-(j). Columns show experiments with different batch sizes.

For LeNet, the weight matrix has the structure

$$\begin{aligned} \text{FC1} &: 256 \times 2450 \\ \text{FC2} &: 2450 \times 500. \end{aligned}$$

As figures 13 and 14 show, the spectra in FC2 are very different under the two training data sets. With MNIST, the spectra in weight matrices are MP type, while with CIFAR10, they are HT type. In FC1, it also displays more regularized structures in LeNet+CIFAR especially in small batch sizes. The weight matrices in MiniAlexNet have the structure

$$\begin{aligned} \text{FC1} &: 4096 \times 384 \\ \text{FC2} &: 384 \times 192. \end{aligned}$$

As figures 15 and 16 show, the spectra in FC1 are very different. In the experiment with CIFAR10, rank collapse appears at the final epoch when the batch size is small, indicating a higher regularization structure.

Different training data sets display different regularization structures, and this takes place independently of the used NNs. In the training of MNIST, both layers in LeNet and MiniAlexNet display a standard MP Law, and the testing accuracy in MNIST achieves 99%. The implied regularization in both NNs is low. In other words, the MNIST data set is in high quality, no intense regularization is needed for the Deep Learning to achieve very high accuracy. In contrary, Heavy Tail appears in both NNs in the training of CIFAR10 data. In LeNet, Heavy Tail appears in FC2 layer and small batch sizes in FC1 layer; In MiniAlexNet, Heavy Tail appears in FC1 layer, and Rank Collapse appears in FC2 when batch size is small. The testing accuracy is only near 75%. In other words, the quality of the CIFAR10 data is not at a perfect level for Deep Learning, high regularization is needed to improve the test accuracy as a compensation for the low quality.

As several researchers have pointed out that SNR is an important indicator in machine learning, such as Support Vector Machine, K-means, and Deep Learning (Thilina et al., 2013; Hossain and Bhargava, 2007; Xie et al., 2020), these experiments establish that the regularization structure is highly affected by the data quality. The Heavy Tail phenomenon reflects a low quality of data or deep learning system. In our numeric and real data experiments, it gives direct evidence on such data-driven regularization.

### 4.3 Early stopping with the spectral criterion

In real data experiments, we still follow the settings in section 3.3 to evaluate the quality of early stopping time using the spectral criterion. Experiment results are shown in Table 5.

**Comments:**

- LeNet+MNIST and LeNet+CIFAR10: Testing accuracy and training accuracy are both increasing during the training process. The FC2 layer in LeNet hits the critical value  $s_*$  first, and provides a time which could stop. For MNIST, the test accuracy in the early stopped epoch only has the negligible difference 0.1% with the final test accuracy; For CIFAR10, the test accuracy is lower but still guaranteed compared with the final test accuracy. We check the FC1 layer for CIFAR10, find that the “strongly suggested” stopping epochs in batch sizes 16 and 32 have much higher test accuracies, and in larger batch sizes, we could stop for saving time or keep training for a higher test accuracy.
- MiniAlexNet+MNIST and MiniAlexNet+CIFAR10: The FC1 layer always hits the critical value first. For MNIST, the test accuracy still has negligible difference with the final test accuracy in small batch sizes 16 and 32, and no early stopping epoch is found by the spectral criterion in large batch sizes. For CIFAR10, it is the most representative experiment because the training explosion happens in batch sizes 16 and 32. We figure out whether spectral criterion gives alarm and performs well. The answer is yes. The spectral criterion strongly suggested to stop before training explosion and has a quite high test accuracy. In large batch sizes, the test accuracies are also ensured with a large amount of cutting training time.

Table 5 shows the robustness and well performance of the spectral criterion. Actually,  $C = 0.4$  makes the critical value quite strict, even generated from MP Law,  $\hat{s}_n n^{\frac{1}{3}} / \sqrt{\log n}$  could achieve the extreme value 0.35, any slight deviation from MP Law could hit the critical value, which we still consider it as MP Law or MPB. We tune the constant  $C = 0.6$  to see what happen. The results are shown in Appendix E.

An interesting thing is that when  $C = 0.6$ , there is nearly no early stopping or training alarm on MNIST, and high quality epochs are still offered in the training of CIFAR10. We also note that with  $C = 0.6$ , the **spectral criterion** predicts the explosion quite accurately in MiniAlexNet+CIFAR10, as the first hit on the critical line is epochs 28 and 188, the explosion begins. (We select epoch 36,196 for smoothness consideration, seen in Figure 17(d) and Table 13.)

**Table 5** Early stopping results in real data experiments with  $C = 0.4$ : stopping epochs selected by spectral criterion in different layers' weight matrices and their testing accuracy (Test Acc). The symbol "-" means no early stopping epoch is found by the spectral criterion.

The combination LeNet+MNIST

batchsize	spectral criterion $C = 0.4$				Final Epoch 248		
	epoch(FC1)	Test Acc	epoch(FC2)	Test Acc	FC1	FC2	Test Acc
16	-		16	99.08%	MP	MPB	99.17%
32	-		40	99.13%	MP	MPB	99.17%
64	-		68	98.98%	MP	MPB	98.98%
128	-		124	98.91%	MP	MP	99.03%
256	-		-		MP	MP	98.96%

The combination LeNet+CIFAR10

batchsize	spectral criterion $C = 0.4$				Final Epoch 248		
	epoch(FC1)	Test Acc	epoch(FC2)	Test Acc	FC1	FC2	Test Acc
16	24	61.37%	8	61.62%	MPB	HT	64.99%
32	60	64.78%	10	57.94%	MP	HT	64.57%
64	-		28	59.19%	MP	HT	62.49%
128	-		60	61.38%	MP	HT	61.83%
256	-		84	54.23%	MP	HT	60.49%

The combination MiniAlexNet+MNIST

batchsize	spectral criterion $C = 0.4$				Final Epoch 248		
	epoch(FC1)	Test Acc	epoch(FC2)	Test Acc	FC1	FC2	Test Acc
16	4	99.23%	-		MPB	MP	99.49%
32	20	99.42%	-		MP	MP	99.41%
64	-		-		MP	MP	99.42%
128	-		-		MP	MP	99.39%
256	-		-		MP	MP	99.31%

The combination MiniAlexNet+CIFAR10

batchsize	spectral criterion $C = 0.4$				Final Epoch 248		
	epoch(FC1)	Test Acc	epoch(FC2)	Test Acc	FC1	FC2	Test Acc
16	3	69.05%	9	72.02%	HT	RC	10%(explode)
32	4	72.17%	16	74.64%	HT	RC	10%(explode)
64	5	71.61%	28	76.35%	HT	MP	77.94%
128	10	74.14%	-		HT	MP	77.43%
256	24	75.70%	-		MPB	MP	75.93%

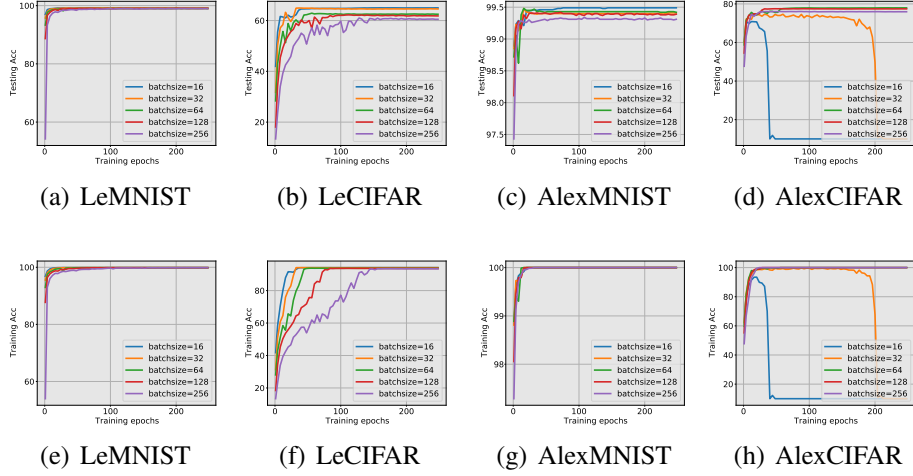


**Figure 17** Testing and Training Accuracy: We begin the line at epoch=1. Testing accuracy: (a)-(d); Training accuracy: (e)-(h). y-axis is the accuracy value, x-axis is the training epochs. Different line represents different SNRs in data sets.

## 5 Other Discussions

### 5.1 Technical details of the spectral criterion

Consider  $n$  data points  $X_1, X_2, \dots, X_n$ , supported on an interval  $[a, b]$ , with  $0 < a < b$ . Consider a mesh net on the interval on  $M$  bins of binsize  $(b - a)/M$ ,

$$B_j = \left( a + (j - 1) \frac{b - a}{M}, a + j \frac{b - a}{M} \right], \quad 1 \leq j \leq M.$$

The histogram estimator for the density function of the data is

$$\hat{p}_M(x) = \frac{M}{n(b - a)} \sum_{i=1}^n I(X_i \in B(x)),$$

$B(x)$  is the bin  $x$  belongs to.

With respect to Random Matrix Theory Results given in Appendix B, the density function of the standard MP Law  $MP_{c,\sigma^2}$  is

$$p_{c,\sigma^2}(x) = MP_{c,\sigma^2}(x) = \frac{1}{2\pi c\sigma^2 x} \sqrt{(b - x)(x - a)},$$

with  $a = \sigma^2(1 - \sqrt{c})^2$  and  $b = \sigma^2(1 + \sqrt{c})^2$ . We thus use the following  $L_1$  distance between the two density functions to measure the departure of the data points  $\{X_i\}$  from

the MP law:

$$s_n = \int_a^b |\hat{p}_M(x) - p_{c,\sigma^2}(x)| dx. \quad (7)$$

We have the following estimated rate for  $s_n$  under the null hypothesis that the data points follow the MP-law.

**Proposition 5.1.** *Suppose  $\{X_i\}_{i=1}^n$  are generated independently from  $p_{c,\sigma^2}(x) = MP_{c,\sigma^2}$ , then the distance in eq7 satisfies*

$$s_n = O_P\left(\frac{1}{M} + \sqrt{\frac{M \log n}{n}}\right).$$

The proof is given in Appendix C.1. Due to the fact that MP density  $p_{c,\sigma^2}(x)$  has unbounded derivatives at its edge points  $\{a, b\}$ , the above estimated rate is obtained via a special adaptation of the existing rate from the literature.

In practice, we do not know the parameters  $c$  and  $\sigma^2$  of the reference MP density  $p_{c,\sigma^2}(x)$ . Then we use the observed extreme statistics  $\hat{a} = X_{(1)}$ , and  $\hat{b} = X_{(n)}$  to estimate  $a$  and  $b$ , respectively. These lead to corresponding estimates  $\hat{c}$  and  $\hat{\sigma}^2$  for the parameters  $c$  and  $\sigma^2$ , respectively. The MP density function with estimated parameters is then

$$p_{\hat{c},\hat{\sigma}^2}(x) = \frac{1}{2\pi\hat{c}\hat{\sigma}^2x} \sqrt{(\hat{b}-x)(x-\hat{a})} I(\hat{a} \leq x \leq \hat{b}).$$

Finally, the  $L_1$  distance between the data set  $\{X_1, \dots, X_n\}$  and the MP law is estimated by

$$\hat{s}_n = \int_a^b |\hat{p}_M(x) - p_{\hat{c},\hat{\sigma}^2}(x)| dx.$$

The following proposition guarantees a convergence rate for the estimator  $\hat{s}_n$ ,

**Proposition 5.2.** *As  $\hat{s}_n$  defined above, we have*

$$\hat{s}_n = O_P\left(\frac{1}{n^{1/3}} + \frac{1}{M} + \sqrt{\frac{M \log n}{n}}\right). \quad (8)$$

The proof of the proposition is given in Appendix C.2.

The proposition is next used to define a rejection region for the null hypothesis. Consider  $M = O(n^{1/3})$ . From (8), under the null hypothesis,  $\hat{s}_n$  will converge to zero at the optimal rate of  $O_P(\sqrt{\log n}/n^{1/3})$ . In contrast, under a deviation of ESDs in weight matrices such as emergence of Heavy Tails,  $\hat{s}_n$  will no longer tend to 0. This result, combined with the previous finding of data-driven regularization in weight matrices spectra, permits the definition of the spectral criterion for early stopping of the training process in a DNN introduced in section 2.3.

**Remark 1.** In the simulation for different MP Laws, we generate eigenvalues and get histograms of  $\hat{s}_n n^{\frac{1}{3}} / \sqrt{\log n}$ . As shown in Figure 18, the value  $\hat{s}_n n^{\frac{1}{3}} / \sqrt{\log n}$  always lies in the interval  $[0.15, 0.25]$ . We empirically suggest the critical line with  $C = 0.4$  from theoretical simulations with comparison to the extreme value 0.35 displayed in Figure 18. The satisfactory results selected by the spectral criterion from  $C = 0.4$  to  $C = 0.6$  are all acceptable in our experiments. Basically, any value of  $C$  in the range of  $[0.4, 0.6]$  can be recommended for the spectral criterion from our experimental results.

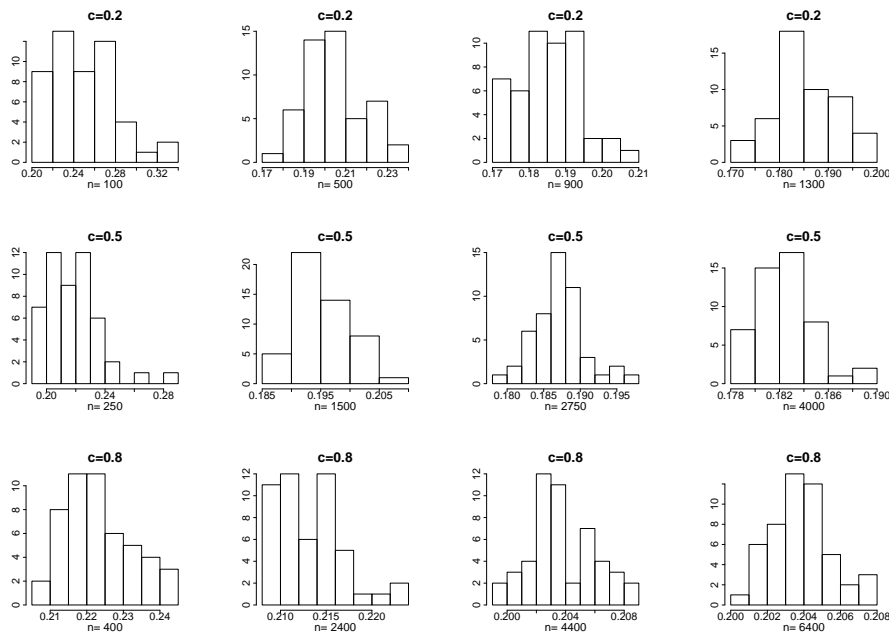


**Figure 18** Histograms of  $\hat{s}_n n^{\frac{1}{3}} / \sqrt{\log n}$  from different  $c$  and  $n$ : For each pair of  $(c, n)$ , the eigenvalues are generated from standard MP Law with 50 repetitions that lead to 50 values of the statistic.

## 5.2 Theoretical Description of state-of-the-art DNNs

As the lack of guidance for such precise theoretical analysis, some researchers believe that practical theories are an alternative choice to guide practice for state-of-the-art DNNs, compared with ideal models for which one proves theorems (Jiang et al., 2020; Martin and Mahoney, 2021; Pappan, 2020). Unlike rigorous theorems proof, which is founded on strict assumptions and mathematical derivation, practical theories are founded on the large amount of numeric or real data experiments. For instance, (Pappan, 2020) attempted to provide a practical explanation of the spikes that emerge in the weight matrices by building a connection to "Between Class covariance". Not only

weight matrices, but he also displays various matrices' spectra such as spectra of Hessian matrices, Feature out covariance matrices and Back Propagation error matrices. All matrices have distant spikes after training dynamics. If one selects ideal models, one may face quite challenging problems to give precise theorems of such phenomena in the theoretical analysis of back propagation.

We thus apply our results to improve the practical theory proposed by (Martin and Mahoney, 2021). In the **Heavy Tail** Period, weight matrices, of which the spectra are shown in Figure 4, are stated as

$$W = W^{rand} + \Delta^{str.corr},$$

where  $\Delta^{str.corr}$  represents strongly correlated "signal" learning during the training process. Martin and Mahoney also points out that  $\Delta^{str.corr}$  can be viewed as a random matrix with entries drawn from a Universal, Heavy Tailed class. In the Heavy Tail period, the degree of self regularization in weight matrices is strong. The **Bulk Transition** Period, which is shown in Figure 5, is the period between Heavy Tail and Light Tail. The bulk in **Bulk Transition** period gradually varies from Heavy Tail to MP Law Bleed Out with increment of SNR. The weight matrices have the form

$$W = W^{rand} + \Delta^{transition},$$

where  $\Delta^{transition}$  is related to SNR. When SNR is low,  $\Delta^{transition}$  is close to the  $\Delta^{str.corr}$  which draw the whole ESD in weight matrix Heavy Tail; When SNR gets higher,  $\Delta^{transition}$  gradually get closer to the structure in Light Tail period. In the **Light Tail** Period, weight matrices, whose spectra are shown in Figure 6, is stated as

$$W = W^{rand} + \Delta^{signal},$$

where  $\Delta^{signal}$  is some moderately large-sized matrix, we may also view  $\Delta^{signal}$  as "signal detection" matrix, that  $\Delta^{signal}$  multiply features to get classification.

We summary the theories, that

$$W = W^{rand} + \Delta(SNR),$$

the regularized structure  $\Delta$  is driven by SNR, with increment of SNR, the regularized  $\Delta$  gradually vary from  $\Delta^{str.corr}$  to  $\Delta^{signal}$ .

### 5.3 Evidence for Data Driven Regularization from matrix ranks

To verify the practical theory description of

$$W = W^{rand} + \Delta(SNR)$$

discussed in Section 5.2, we focus on the spectra types. From the matrix ranks, we still validate the theoretical description of weight matrices. As data SNR increases, the value of spikes in the weight matrix decrease. We use the MP-soft rank defined below to measure the sharpness of distant spikes. Figure 19 shows that the sharpness of spikes is reduced, and the distance between spikes and bulk is closer as SNR increases.

**MP-soft Rank:** Identify the bulk edge  $\lambda^+$  and the maximum value of eigenvalues  $\lambda_{\max}$ , the soft rank is defined as

$$\text{MP-soft Rank: } R_{\text{Sf}} = \frac{\lambda^+}{\lambda_{\max}} \in (0, 1]$$

**MP-stable Rank:**  $\lambda_i$  is the eigenvalue of  $W^T W$ , the stable rank is defined as

$$\text{MP-stable Rank: } R_{\text{St}} = \frac{\sum_i \lambda_i}{\lambda_{\max}} \in (1, +\infty)$$

The MP-soft Rank measures how the sharp spikes deviated from the bulk, and the MP-stable Rank is the well-known discounted dimension of the weight matrix. Beyond the empirically observed threshold, as SNR grows, MP-soft rank and MP-stable Rank grow as Figure 19 shown. In the particular view of eigenvalues, the largest spike of weight matrix in all layers becomes closer to the bulk when we enlarge SNR. SNR in the training data drives the change of implicit regularization in the whole weight matrix from the rank perspective. It remains questions on why the increment of SNR makes the gap between the spikes and bulk smaller, and theorists also face the question on the threshold above which the ranks increase.

## 6 Conclusion

By studying the spectra of weight matrices in trained DNNs, we find a connection between their types and the ongoing regularization. Further, we establish the evidence that the implicit regularization in the network is data-driven, controlled by the quality of the training data. Such implicit data driven regularization in the weight matrices provides a new way of understanding the whole training procedure. We apply this phenomenon to derive an early stopping procedure in order to avoid over-training (in case of poor data quality). This study also leads to several questions to explore in the future, such as the explanation of the number of spikes and how SGD generates Heavy Tail in the poor data quality but Light Tail in the high data quality in DNNs.

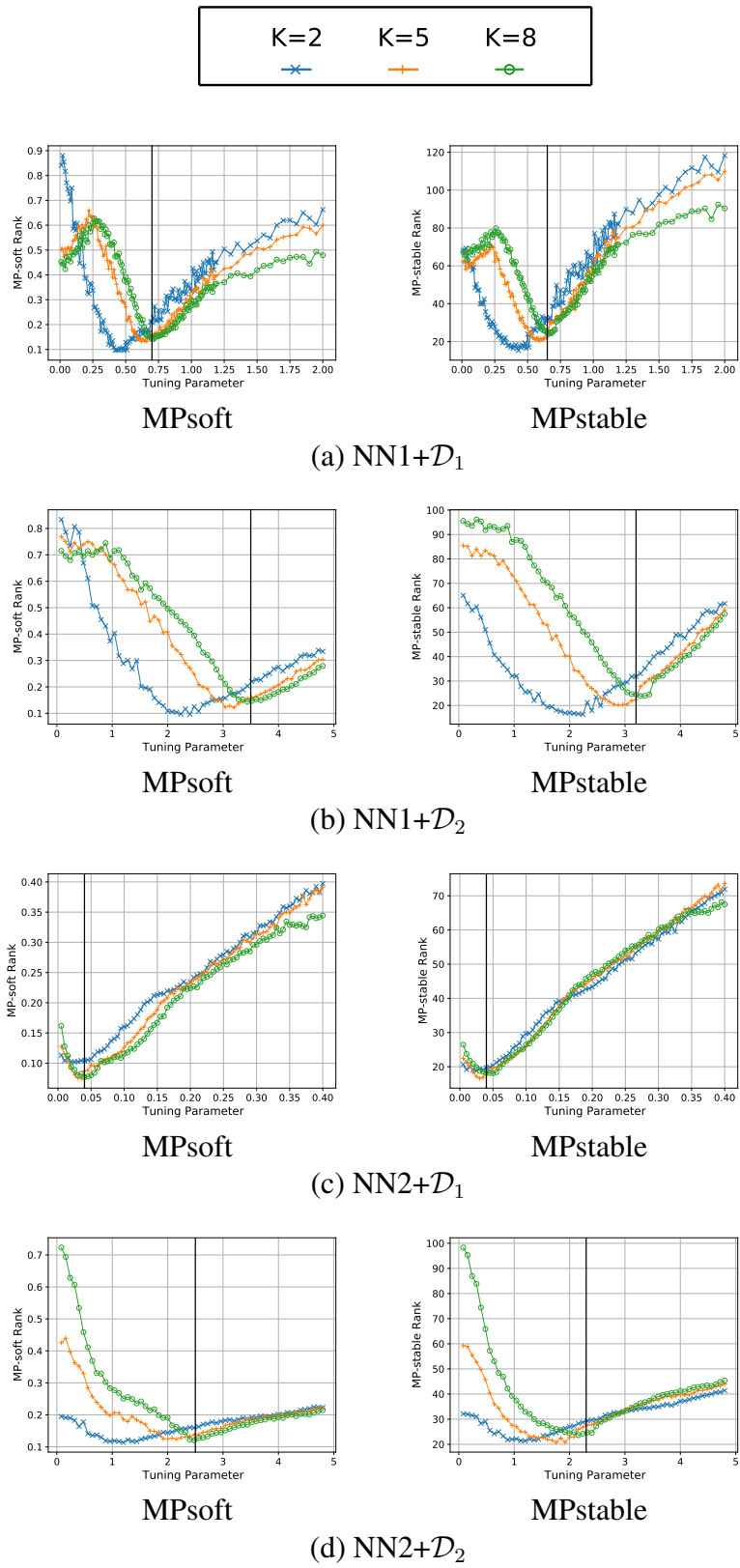


**Figure 19** The Rank of weight matrix in FC2 at final epoch 248. The solid line is the threshold.  $x$ -axis is the tuning parameter proportional to SNR,  $y$ -axis is the well-defined Rank.

## References

- Yann LeCun, Yoshua Bengio, and Geoffrey Hinton. Deep learning. *nature*, 521(7553): 436–444, 2015.
- Yann Dauphin, Razvan Pascanu, Caglar Gulcehre, Kyunghyun Cho, Surya Ganguli, and Yoshua Bengio. Identifying and attacking the saddle point problem in high-dimensional non-convex optimization, 2014.
- Vardan Papyan. The full spectrum of deepnet Hessians at scale: Dynamics with SGD training and sample size, 2019a.
- Vardan Papyan. Measurements of three-level hierarchical structure in the outliers in the spectrum of deepnet Hessians. *CoRR*, abs/1901.08244, 2019b. URL <http://arxiv.org/abs/1901.08244>.
- Levent Sagun, Leon Bottou, and Yann LeCun. Eigenvalues of the Hessian in deep learning: Singularity and beyond, 2017.
- Zhewei Yao, Amir Gholami, Kurt Keutzer, and Michael W. Mahoney. PyHessian: Neural networks through the lens of the Hessian. In *2020 IEEE International Conference on Big Data (Big Data)*, pages 581–590, 2020. doi: 10.1109/BigData50022.2020.9378171.
- Diego Granzio. Beyond random matrix theory for deep networks, 2020.
- Jeffrey Pennington and Pratik Worah. Nonlinear random matrix theory for deep learning. *Journal of Statistical Mechanics: Theory and Experiment*, 2019(12):124005, dec 2019. doi: 10.1088/1742-5468/ab3bc3. URL <https://doi.org/10.1088/1742-5468/ab3bc3>.
- Jungang Ge, Ying-Chang Liang, Zhidong Bai, and Guangming Pan. Large-dimensional random matrix theory and its applications in deep learning and wireless communications, 2021.
- Charles H. Martin and Michael W. Mahoney. Implicit self-regularization in deep neural networks: Evidence from random matrix theory and implications for learning. *Journal of Machine Learning Research*, 22(165):1–73, 2021. URL <http://jmlr.org/papers/v22/20-410.html>.
- Jan Kuckacka, Vladimir Golkov, and Daniel Cremers. Regularization for deep learning: A taxonomy, 2017.
- Mert Gurbuzbalaban, Umut Şimşekli, and Lingjiong Zhu. The heavy-tail phenomenon in SGD, 2021.

- Jaehoon Lee, Jascha Sohl-dickstein, Jeffrey Pennington, Roman Novak, Sam Schoenholz, and Yasaman Bahri. Deep neural networks as gaussian processes. In *International Conference on Learning Representations*, 2018. URL <https://openreview.net/forum?id=B1EA-M-0Z>.
- Yann LeCun, Léon Bottou, Yoshua Bengio, and Patrick Haffner. Gradient-based learning applied to document recognition. *Proceedings of the IEEE*, 86(11):2278–2324, 1998.
- Alex Krizhevsky, Ilya Sutskever, and Geoffrey E Hinton. Imagenet classification with deep convolutional neural networks. *Advances in neural information processing systems*, 25:1097–1105, 2012.
- Charles H Martin, Tongsu Serena Peng, and Michael W Mahoney. Predicting trends in the quality of state-of-the-art neural networks without access to training or testing data. *Nature Communications*, 12(1):1–13, 2021.
- Vardan Papyan, XY Han, and David L Donoho. Prevalence of neural collapse during the terminal phase of deep learning training. *Proceedings of the National Academy of Sciences*, 117(40):24652–24663, 2020.
- Wenlong Ji, Yiping Lu, Yiliang Zhang, Zhun Deng, and Weijie J Su. How gradient descent separates data with neural collapse: A layer-peeled perspective. 2021.
- Nitish Shirish Keskar, Dheevatsa Mudigere, Jorge Nocedal, Mikhail Smelyanskiy, and Ping Tak Peter Tang. On large-batch training for deep learning: Generalization gap and sharp minima. *CoRR*, abs/1609.04836, 2016. URL <http://arxiv.org/abs/1609.04836>.
- Priya Goyal, Piotr Dollár, Ross B. Girshick, Pieter Noordhuis, Lukasz Wesolowski, Aapo Kyrola, Andrew Tulloch, Yangqing Jia, and Kaiming He. Accurate, large minibatch SGD: training imagenet in 1 hour. *CoRR*, abs/1706.02677, 2017. URL <http://arxiv.org/abs/1706.02677>.
- Karaputugala Madushan Thilina, Kae Won Choi, Nazmus Saquib, and Ekram Hossain. Machine learning techniques for cooperative spectrum sensing in cognitive radio networks. *IEEE Journal on selected areas in communications*, 31(11):2209–2221, 2013.
- Ekram Hossain and Vijay K Bhargava. *Cognitive wireless communication networks*. Springer Science and Business Media, 2007.
- Xiaojuan Xie, Shengliang Peng, and Xi Yang. Deep learning-based signal-to-noise ratio estimation using constellation diagrams. *Mobile Information Systems*, 2020, 2020.

Yiding Jiang, Pierre Foret, Scott Yak, Daniel M. Roy, Hossein Mobahi, Gintare Karolina Dziugaite, Samy Bengio, Suriya Gunasekar, Isabelle Guyon, and Behnam Neyshabur. Neurips 2020 competition: Predicting generalization in deep learning, 2020.

Vardan Papyan. Traces of class/cross-class structure pervade deep learning spectra, 2020.

Jianfeng Yao, Shurong Zheng, and ZD Bai. *Sample covariance matrices and high-dimensional data analysis*. Cambridge University Press Cambridge, 2015.

# **Supplementary materials to ‘Implicit Data-Driven Regularization in Deep Neural Networks under SGD’**

Xuran Meng, Jianfeng Yao

*Department of Statistics and Actuarial Science, University of Hong Kong,  
Hong Kong SAR, China*

\* *To whom correspondence should be addressed: [jeffyao@hku.hk](mailto:jeffyao@hku.hk)*

## A Numeric Experiments

**Table 6**  $NN2+D_1$ : The results of ESD types in different layers with different SNR, and the number of spikes is related to Classes number.

Classes Number	Layer	Transition Period	TP Range+ESD Type
K=2	FC1	Heavy Tail	[0.005-0.015]: HT(0,1)
		Bulk Transition	[0.02-0.055]: HT(1,1)→MPB(1,1)
		Light Tail	[0.06,0.235]: MP(1,1) [0.24,0.4]: MP(0,1)
	FC2	Heavy Tail	-
		Bulk Transition	-
		Light Tail	[0.005,0.4]: MP(1,1)
K=5	FC1	Heavy Tail	[0.005,0.015]: HT(0,1) [0.02,0.035]: HT(4,1) [0.04,0.045]: HT(0,5)
		Bulk Transition	[0.05,0.12]: HT(1,4)→MPB(1,4)
		Light Tail	[0.125,0.4]: MP(1,4)
	FC2	Heavy Tail	-
		Bulk Transition	[0.005,0.025]: HT(1,4)→MPB(1,4)
		Light Tail	[0.03,0.38]: MP(1,4) [0.385,0.4]: MP(0,5)
K=8	FC1	Heavy Tail	[0.005,0.025]: HT(0,1) [0.03,0.06]: HT(7,1) [0.065]: HT(0,8)
		Bulk Transition	[0.07,0.135]: HT(1,7)→MPB(1,7)
		Light Tail	[0.135,0.4]: MP(1,7)
	FC2	Heavy Tail	-
		Bulk Transition	[0.005,0.095]: MPB(1,7)
		Light Tail	[0.1,0.24]: MP(1,7) [0.245,0.4]: MP(0,8)

**Table 7**  $NN2+D_2$ : The results of ESD types in different layers with different SNR, and the number of spikes is related to Classes number.

Classes Number	Layer	Transition Period	TP Range+ESD Type
K=2	FC1	Heavy Tail	[0.08,0.16]: HT(0,1)
		Bulk Transition	[0.24-1.52]: HT(1,1)→MPB(1,1)
		Light Tail	[1.6,1.92]: MP(1,1) [2,4.8]: MP(0,1)
	FC2	Heavy Tail	-
		Bulk Transition	[0.08,0.48]: MPB(1,1)
		Light Tail	[0.56,4.8]: MP(0,1)
K=5	FC1	Heavy Tail	[0.08,0.48]: HT(0,0) [0.56]: HT(0,1) [0.64,0.88]: HT(0,5)
		Bulk Transition	[0.96,2.24]: HT(1,4)→MPB(1,4)
		Light Tail	[2.32,2.48]: MP(1,4) [2.56,4.8]: MP(0,4)
	FC2	Heavy Tail	-
		Bulk Transition	[0.08,2.16]: HT(0,4) → MPB(1,4)
		Light Tail	[2.24,4.8]: MP(1,4)
K=8	FC1	Heavy Tail	[0.08,0.96]: HT(0,0) [1.04,1.12]: HT(0,8)
		Bulk Transition	[1.2,2.72]: HT(1,7)→MPB(1,7)
		Light Tail	[2.8,3.04]: MP(1,7) [3.12,4.8]: MP(0,7)
	FC2	Heavy Tail	-
		Bulk Transition	[0.08,2.4]:HT(0,7)→ MPB(1,7)
		Light Tail	[2.48,4.8]: MP(1,7)→MP(0,8)

**Table 8**  $NN1+D_1$ : The results of ESD types in different layers with different SNR.

Classes Number	Layer	Transition Period	TP Range+ESD Type
K=2	FC2	Heavy Tail	[0.01,0.03]: HT(0,1) [0.04-0.09]: HT(0,2)
		Bulk Transition	[0.1-0.44]: HT(1,1)→MPB(1,1)
		Light Tail	[0.45-2]: MP(1,1)
	FC3	Heavy Tail	-
		Bulk Transition	[0.01,0.29]: MPB(1,1)
		Light Tail	[0.3,0.38]: MP(1,1) [0.39,2]: MP(0,1)
	FC4	Heavy Tail	-
		Bulk Transition	-
		Light Tail	[0.01,2]: MP(0,1)
K=5	FC2	Heavy Tail	[0.01,0.15]: HT(0,1) [0.16,0.2]: HT(4,1) [0.2,0.28]: HT(0,5)
		Bulk Transition	[0.28,0.66]: HT(1,4)→MPB(1,4)
		Light Tail	[0.67,1.04]: MP(1,4) [1.04,2]: MP(0,5)
	FC3	Heavy Tail	-
		Bulk Transition	[0.01,0.59]: HT(1,4)→MPB(1,4)
		Light Tail	[0.6,1.9]: MP(1,4) [1.95,2]: MP(0,5)
	FC4	Heavy Tail	-
		Bulk Transition	-
		Light Tail	[0.01,2]: MP(0,4)
K=8	FC2	Heavy Tail	[0.01,0.19]: HT(0,1) [0.2,0.25]: HT(7,1) [0.26,0.36]: HT(0,8)
		Bulk Transition	[0.37-0.72]: HT(1,7)→MPB(1,7)
		Light Tail	[0.73,1.01]: MP(1,7) [1.02,1.9]: MP(0,8) [1.95,2]: MP(0,7)
	FC3	Heavy Tail	[0.01,0.32]: HT(0,8)
		Bulk Transition	[0.32,0.62]: HT(1,7)→MPB(1,7)
		Light Tail	[0.63,1.15]: MP(1,7) [1.16,1.95]: MP(0,8) [2]: MP(0,7)
	FC4	Heavy Tail	-
		Bulk Transition	-
		Light Tail	[0.01,2]: MP(0,7)

**Table 9**  $NN1+D_2$ : The results of ESD types in different layers with different SNR.

Classes Number	Layer	Transition Period	TP Range+ESD Type
K=2	FC2	Heavy Tail	[0.08,0.024]: HT(0,1) [0.32,0.4]: HT(0,2)
		Bulk Transition	[0.48-2.16]: HT(1,1)→MPB(1,1)
		Light Tail	[2.24,4.8]: MP(1,1)
	FC3	Heavy Tail	-
		Bulk Transition	[0.08,1.44]: HT(1,1)→MPB(1,1)
		Light Tail	[1.52,2.64]: MP(1,1) [2.72,4.8]: MP(0,1)
	FC4	Heavy Tail	-
		Bulk Transition	-
		Light Tail	[0.08,4.8]: MP(0,1)
K=5	FC2	Heavy Tail	[0.08,0.48]: HT(0,1) [0.56,0.64]: HT(4,1) [0.72,1.04]: HT(0,5)
		Bulk Transition	[1.12,3.2]: HT(1,4)→MPB(1,4)
		Light Tail	[3.28,4.8]: MP(1,4)
	FC3	Heavy Tail	-
		Bulk Transition	[0.08,2.72]: HT(1,4)→MPB(1,4)
		Light Tail	[2.8,4.8]: MP(1,4)
	FC4	Heavy Tail	-
		Bulk Transition	-
		Light Tail	[0.08,4.8]: MP(0,4)
K=8	FC2	Heavy Tail	[0.08,0.56]: HT(0,1) [0.64,0.96]: HT(7,1) [1.04,1.36]: HT(0,8)
		Bulk Transition	[1.44,3.52]: HT(1,7)→MPB(1,7)
		Light Tail	[3.6,4.64]: MP(1,7) [4.8]: MP(0,8)
	FC3	Heavy Tail	[0.08,1.12]: HT(7,1) [1.12,1.44]: HT(0,8)
		Bulk Transition	[1.52,3.12]: HT(1,7)→MPB(1,7)
		Light Tail	[3.12,4.8]: MP(1,7)
	FC4	Heavy Tail	-
		Bulk Transition	-
		Light Tail	[0.08,4.8]: MP(0,7)

**Table 10**  $NN1+\mathcal{D}_1$ : The results in different batch sizes. RC means Rank Collapse.

Batch Size	Layer	Transition Period	TP Range+ESD Type
256	FC2	Heavy Tail	[0.01,0.16]: HT(0,0) [0.17,0.22]: HT(0,8)
		Bulk Transition	[0.23,0.55]: HT(0,7)→MPB(0,7)
		Light Tail	[0.56,2]: MP(1,7)
	FC3	Heavy Tail	-
		Bulk Transition	[0.01,0.4]: MPB(1,7)
		Light Tail	[0.41,1.01]: MP(1,7) [1.02,1.95]: MP(0,8) [2]: MP(0,7)
	FC4	Heavy Tail	-
		Bulk Transition	-
		Light Tail	[0.01,2]: MP(0,7) (RC→MP)
64	FC2	Heavy Tail	[0.01,0.19]: HT(0,1) [0.2,0.25]: HT(7,1) [0.26,0.36]: HT(0,8)
		Bulk Transition	[0.37-0.72]: HT(1,7)→MPB(1,7)
		Light Tail	[0.73,1.09]: MP(1,7) [1.1,1.9]: MP(0,8) [1.95,2]: MP(0,7)
	FC3	Heavy Tail	[0.01,0.32]: HT(0,8)
		Bulk Transition	[0.32,0.62]: HT(1,7)→MPB(1,7)
		Light Tail	[0.63,1.15]: MP(1,7) [1.16,1.95]: MP(0,8) [2]: MP(0,7)
	FC4	Heavy Tail	-
		Bulk Transition	-
		Light Tail	[0.01,2]: MP(0,7) (RC→MP)
32	FC2	Heavy Tail	[0.01,0.17]: HT(0,1) [0.18,0.46]: HT(7,1) [0.47,0.55]: HT(0,8)
		Bulk Transition	[0.56,0.8]: HT(1,7)→MPB(0,7)
		Light Tail	[0.81,0.84]: MP(0,7) [0.85,1.08]: MP(1,7) [1.09,2]: MP(0,8)
	FC3	Heavy Tail	[0.01,0.44]: RC [0.45,0.52]: HT(7,1) [0.53,0.59]: HT(0,8)
		Bulk Transition	[0.6,0.72]: HT(1,7)→MPB(0,7)
		Light Tail	[0.73,0.78]: MP(0,7) [0.79,1.12]: MP(1,7) [1.13,2]: MP(0,8)
	FC4	Heavy Tail	-
		Bulk Transition	[0.01,0.45]: HT(0,7)→MPB(0,7) (RC)
		Light Tail	[0.46,2]: MP(0,7) (RC→MP)

**Table 11** NN2+ $\mathcal{D}_2$ : The results in different batch sizes.

Batch Size	Layer	Transition Period	TP Range+ESD Type
256	FC1	Heavy Tail	-
		Bulk Transition	-
		Light Tail	[0.08,1.2]: MP(0,0) [1.28,4.8]: MP(0,7)
	FC2	Heavy Tail	-
		Bulk Transition	-
		Light Tail	[0.08,4.64]: MP(1,7) [4.72,4.8]: MP(0,8)
64	FC1	Heavy Tail	[0.08,0.96]: HT(0,0) [1.04,1.12]: HT(0,8)
		Bulk Transition	[1.2,2.72]: HT(1,7)→MPB(1,7)
		Light Tail	[2.8,3.04]: MP(1,7) [3.12,4.8]: MP(0,7)
	FC2	Heavy Tail	-
		Bulk Transition	[0.08,2.4]: MPB(1,7)
		Light Tail	[2.48,4.8]: MP(1,7)→MP(0,8)
32	FC1	Heavy Tail	[0.08,0.8]: HT(0,0)
		Bulk Transition	[0.88,3.6]: HT(0,7)→MPB(0,7)
		Light Tail	[3.68,4.8]: MP(0,7)
	FC2	Heavy Tail	-
		Bulk Transition	[0.08,3.28]: RC→MPB(0,7)
		Light Tail	[3.36,4.8]: MP(1,7)

## B Preliminaries on RMT

In this section, we review the results we use from RMT. RMT provides us lots of analysis results for both square or rectangular large matrices. The well-known results in RMT: Marchenko-Pauster (MP) Law which shows eigenvalues' distribution of rectangular matrices, and Tracy-Widom Law which describes how the max eigenvalue distributed. When analyze DNNs weight matrices, MP Law, which is applicable to rectangular matrices, will give guidance on the analysis in spectrum of DNNs weight matrices.

### B.1 MP Law and stieltjes Transform

MP Law is given as follows,

**Theorem B.1.** (*Marchenko Pauster Law*) Suppose that the entries  $\{w_{ij}\}$  of the matrix  $W \in \mathbb{R}^{n \times p}$  are i.i.d. complex random variables with mean zero and variance  $\sigma^2$ , and  $n/p \rightarrow c \in (0, \infty)$ . Define  $S_p = \frac{1}{p}WW^*$ ,  $\lambda_1 \geq \lambda_2 \geq \dots \geq \lambda_n$  is the eigenvalue of  $S_p$ , then the ESD of  $S_p$

$$F^{S_p} \triangleq \frac{1}{n} \sum_j I(x < \lambda_j) \xrightarrow{a.s.} F_{c,\sigma^2}(x)$$

as  $p \rightarrow \infty$ , here  $I(\cdot)$  is the indicator function,  $F_{c,\sigma^2}$  is the MP Law has the form

$$F_{c,\sigma^2}(x) = \begin{cases} \frac{1}{2\pi xc\sigma^2} \sqrt{(b-x)(x-a)}, & \text{if } a \leq x \leq b, \\ 0, & \text{otherwise,} \end{cases}$$

with an additional point mass of value  $1 - 1/c$  at the origin if  $c > 1$ , where  $a = \sigma^2(1 - \sqrt{c})^2$  and  $b = \sigma^2(1 + \sqrt{c})^2$ .

The powerful mathematical tool to achieve the MP Law is stieltjes Transform, let  $\nu$  be a finite measure on the real line with support  $\Gamma_\nu$ , its stieltjes transform is

$$s_\nu(z) = \int \frac{1}{x-z} \nu(dx), \quad z \in \mathbb{C} \setminus \Gamma_\nu.$$

To reduce  $\nu$  from Stieltjes transform, we have the equation

$$\nu(x) = \lim_{v \rightarrow 0^+} \frac{1}{\pi} \Im s_\nu(x + iv).$$

Details can be referred in (Yao et al., 2015).

The Stieltjes transform of standard MP Law satisfies equation

$$s(z) = \frac{1}{1 - z - \{c + czs(z)\}},$$

we can get results in a more generalized settings:

**Theorem B.2.** (*Generalized MP Law*) Let  $S_p$  be the matrix defined in Theorem B.1,  $(T_p)$  is a sequence of nonnegative Hermitian matrices of size  $n \times n$  which is deterministic or independent with  $S_p$ , and the sequence  $(H_p = F^{T_p})$  of the ESD of  $(T_p)$  almost surely weakly converges to a nonrandom probability measure  $H(t)$ , then the ESD  $(F^{S_p T_p})$  of  $S_p T_p$  weakly converges to a nonrandom probability measure  $F_{c,H}$ , that its Stieltjes transform is implicitly defined by the equation

$$s(z) = \int \frac{1}{t(1 - c - czs(z)) - z} dH(t), \quad z \in \mathbb{C}^+$$

## B.2 Spike Model

Suppose that the matrix  $T_p$  has the limit ESD  $H(t)$ , the element  $w_{ij}$  in  $W$  satisfies

$$Ew_{11} = 0, Ew_{11}^2 = 1, Ew_{11}^4 < +\infty$$

define

$$\psi(\alpha) = \psi_{c,H}(\alpha) = \alpha + c \int \frac{t\alpha}{\alpha - t} dH(t),$$

we say the eigenvalue  $\alpha_j$  of  $T_p$  with fixed index  $j$  is a distant spike eigenvalue if

$$\psi'(\alpha_j) > 0.$$

Then we have the following theorem,

**Theorem B.3.** *The entries  $\{w_{ij}\}$  of the matrix  $W \in \mathbb{R}^{n \times p}$  are i.i.d. complex random variables with mean zero, variance 1 and finite fourth moment,  $n/p \rightarrow c \in (0, \infty)$ .  $S_p = \frac{1}{p}WW^*$ ,  $(T_p)$  is a sequence of nonnegative Hermitian matrices of size  $n \times n$  which is deterministic or independent with  $S_p$ , and the sequence  $(H_p = F^{T_p})$  of the ESD of  $(T_p)$  almost surely weakly converges to a nonrandom probability measure  $H(t)$ ,  $\lambda_1 \geq \lambda_2 \geq \dots \geq \lambda_n$  is the eigenvalue of  $S_p T_p$ ,  $\alpha_1 \geq \alpha_2 \geq \dots \geq \alpha_n$  is the eigenvalue of  $T_p$ , suppose that  $\alpha_j$  with fixed index  $j$  is a distant spike eigenvalue, then as  $p \rightarrow +\infty$ , (1) if  $\alpha_1 < +\infty$ , then  $\lambda_j \xrightarrow{a.s.} \psi(\alpha_j)$ ,*

*(2) if  $\alpha_j \rightarrow +\infty$ , then  $\lambda_j/\alpha_j \xrightarrow{a.s.} 1$ .*

## B.3 Tracy-Widom Law

**Theorem B.4.** (*Tracy-Widom Law*) Let  $\{w_{i,j}\}$ ,  $i, j = 1, 2, \dots$ , be a double array of i.i.d. complex-valued random variables with mean 0, variance 1 and finite fourth-order

moment. Consider the sample covariance matrix  $S_p$  defined same as Theorem B.1, the eigenvalues of  $S_p$ :  $\lambda_1 \geq \lambda_2 \geq \dots \geq \lambda_n$  in a decreasing order. When  $n/p \rightarrow c$ , we have

$$\lambda_1 \xrightarrow{a.s.} (1 + \sqrt{c})^2, \quad (\text{order } 0)$$

further, define  $\mu_{pn} = \frac{1}{p} \{(p-1)^{\frac{1}{2}} + n^{\frac{1}{2}}\}^2$  and  $\sigma_{pn} = \frac{1}{p} [(p-1)^{\frac{1}{2}} + n^{\frac{1}{2}}] \{(p-1)^{-\frac{1}{2}} + n^{-\frac{1}{2}}\}^{\frac{1}{3}}$ ,

$$\frac{\lambda_1 - \mu_{pn}}{\sigma_{pn}} \xrightarrow{d} F_1, \quad (\text{order } 1)$$

where  $F_1$  is the Tracy-Widom Law of order 1 whose distribution function is given by

$$F_1(s) = \exp \left\{ \int_s^{+\infty} q(x) + (x-s)^2 q^2(x) dx \right\}, \quad s \in \mathbb{R},$$

where  $q$  solves the Painleve II differential equation

$$q''(x) = xq(x) + 2q^3(x).$$

## C proof

### C.1 Proof of proposition 5.1

$$\begin{aligned} s_n &= \int_a^b |\hat{p}_M(x) - p(x)| dx \\ &\leq \int_a^b |E\hat{p}_M(x) - p(x)| dx + \int_a^b |\hat{p}_M(x) - E\hat{p}_M(x)| dx \end{aligned}$$

Recall

$$\hat{p}_M(x) = \frac{M}{n(b-a)} \sum_{i=1}^n I(X_i \in B(x)).$$

◦ If  $x \in B_1 \cup B_M$ , for simplicity, we assume  $x \in B_1$ , then

$$\begin{aligned} P(X_i \in B_1) &= C \int_a^{a+\frac{b-a}{M}} \frac{\sqrt{(b-x)(x-a)}}{x} dx \\ &= C * \frac{b-a}{M} * \frac{\sqrt{(b-x^*)(x^*-a)}}{x^*} \\ &\leq C * \frac{1}{M} * \sqrt{\frac{1}{M}} \\ &= O\left(\frac{1}{M^{\frac{3}{2}}}\right) \end{aligned}$$

Same to get  $P(X_i \in B_M) = O\left(\frac{1}{M^{\frac{3}{2}}}\right)$ . It is obviously to get that

$$\begin{aligned} \int_{B_1 \cup B_M} |E\hat{p}_M(x) - p(x)| dx &\leq \int_{B_1 \cup B_M} E\hat{p}_M(x) + p(x) dx \\ &= \int_{B_1 \cup B_M} \frac{M}{b-a} P(X_i \in B_1 \cup B_M) dx + P(X_i \in B_1 \cup B_M) \\ &= O\left(\frac{1}{M^{\frac{3}{2}}}\right) \end{aligned}$$

◦ If  $x \notin B_1 \cup B_M$ , assume that  $x \in B_l$ ,  $l \in \{2, 3, \dots, M-1\}$ , note

$$\begin{aligned} E\hat{p}_M(x) &= \frac{M}{b-a} P(X_i \in (B(x))) \\ &= \frac{\int_{a+\frac{l}{M}(b-a)}^{a+\frac{l+1}{M}(b-a)} p(u) du}{(b-a)/M} \\ &= p(x^*), \end{aligned}$$

where  $x^* \in B_l$ . We have for  $\forall x \in B_l$ ,

$$\begin{aligned}
|E\hat{p}_M(x) - p(x)| &= |p(x^*) - p(x)| \\
&\leq |p'(x^{**})(x^* - x)| \\
&\leq C * \frac{|x^{**} - (x^{**} - a)(b - x^{**})|}{\sqrt{(x^{**} - a)(b - x^{**})(x^{**})^2}} * |x^* - x| \\
&= O\left(\sqrt{\frac{M}{l}}\right) * O\left(\frac{1}{M}\right) = \frac{1}{\sqrt{lM}}
\end{aligned}$$

Then

$$\begin{aligned}
\int_{B_1^C \cap B_M^C} |E\hat{p}_M(x) - p(x)| dx &= \sum_{l=2}^{M-1} \int_{B_l} |E\hat{p}_M(x) - p(x)| dx \\
&\leq \sum_{l=2}^{M-1} \int_{B_l} \frac{1}{\sqrt{l}} \cdot O\left(\frac{1}{\sqrt{M}}\right) dx \\
&= \sum_{l=2}^{M-1} \frac{1}{\sqrt{l}} \cdot O\left(\frac{1}{\sqrt{M}}\right) \cdot \frac{1}{M} \\
&= O\left(\frac{1}{M}\right)
\end{aligned}$$

Thus

$$\begin{aligned}
\int_a^b |E\hat{p}_M(x) - p(x)| dx &= \int_{B_1 \cup B_M} |E\hat{p}_M(x) - p(x)| dx \\
&\quad + \int_{B_1^C \cap B_M^C} |E\hat{p}_M(x) - p(x)| dx \\
&= O\left(\frac{1}{M}\right)
\end{aligned}$$

For the part  $\int_a^b |\hat{p}_M(x) - E\hat{p}_M(x)| dx$ , we have

$$\begin{aligned}
P\left(\sup_x |\hat{p}_M(x) - E\hat{p}_M(x)| > \varepsilon\right) &= P\left(M \cdot \max_{l=1, \dots, M} \frac{1}{n} \left| \sum_{i=1}^n I(X_i \in B_l) - nP(X_i \in B_l) \right| > \varepsilon\right) \\
&= P\left(\max_{l=1, \dots, M} \frac{1}{n} \left| \sum_{i=1}^n I(X_i \in B_l) - nP(X_i \in B_l) \right| > \frac{\varepsilon}{M}\right) \\
&\leq \sum_{l=1}^M P\left(\frac{1}{n} \left| \sum_{i=1}^n I(X_i \in B_l) - nP(X_i \in B_l) \right| > \frac{\varepsilon}{M}\right)
\end{aligned}$$

Note that  $P(X_i \in B_l) = O(1/M)$ , by Bernstein inequality,

$$\begin{aligned} \sum_{l=1}^M P\left(\frac{1}{n} \left| \sum_{i=1}^n I(X_i \in B_l) - nP(X_i \in B_l) \right| > \frac{\varepsilon}{M}\right) &\leq \sum_{l=1}^M e^{-C \frac{n^2 \varepsilon^2}{M + 3M}} \\ &\leq M e^{-C \frac{n\varepsilon}{M}} \end{aligned}$$

for some constant  $C > 0$ , set  $\varepsilon = \sqrt{\frac{M \log n}{n}}$ , we achieve

$$\sup_{x \in [a, b]} |\hat{p}_M(x) - E\hat{p}_M(x)| = O_P\left(\sqrt{\frac{M \log n}{n}}\right),$$

which implies for  $\forall$  given  $\varepsilon > 0$ , there  $\exists R > 0$ , such that

$$P\left(\sqrt{\frac{n}{M \log n}} \sup_{x \in [a, b]} |\hat{p}_M(x) - E\hat{p}_M(x)| > R\right) < \varepsilon,$$

for  $\int_a^b |\hat{p}_M(x) - E\hat{p}_M(x)| dx$ , there exists  $x_n$  such that

$$|\hat{p}_M(x_n) - E\hat{p}_M(x_n)|(b-a) \geq \int_a^b |\hat{p}_M(x) - E\hat{p}_M(x)| dx,$$

then

$$\begin{aligned} \varepsilon &> P\left(\sqrt{\frac{n}{M \log n}} \sup_{x \in [a, b]} |\hat{p}_M(x) - E\hat{p}_M(x)| > R\right) \\ &\geq P\left(\sqrt{\frac{n}{M \log n}} |\hat{p}_M(x_n) - E\hat{p}_M(x_n)|(b-a) > R(b-a)\right) \\ &\geq P\left(\sqrt{\frac{n}{M \log n}} \int_a^b |\hat{p}_M(x) - E\hat{p}_M(x)| dx > R(b-a)\right) \end{aligned}$$

Thus we achieve

$$\int_a^b |\hat{p}_M(x) - E\hat{p}_M(x)| dx = O_P\left(\sqrt{\frac{M \log n}{n}}\right),$$

which proves the proposition.

## C.2 Proof of proposition 5.2

For  $\forall \varepsilon > 0, \exists R > 0$  such that

$$\begin{aligned}
P(n^{\frac{2}{3}}(X_{(1)} - a) > R) &= \prod_{i=1}^n P(X_i - a > R/n^{\frac{2}{3}}) \\
&= (1 - \int_a^{a + \frac{R}{n^{\frac{2}{3}}}} p(x) dx)^n \\
&\sim (1 - C \int_a^{a + \frac{R}{n^{\frac{2}{3}}}} \sqrt{x - a} dx)^n \\
&= (1 - CR^{\frac{3}{2}}/n)^n \\
&< \varepsilon
\end{aligned}$$

as  $n \rightarrow \infty$ , then  $X_{(1)} - a = O_P(n^{-\frac{2}{3}})$ , similar to get  $b - X_{(n)} = O_P(n^{-\frac{2}{3}})$ , which implies same rate as Tracy Widom Law.

$$\hat{s}_n \leq s_n + \int_a^b |\hat{p}(x) - p(x)| dx,$$

then we prove that

$$\int_a^b |\hat{p}(x) - p(x)| dx = O_P(n^{-\frac{1}{3}}).$$

Indeed, set  $C_0 = 2\pi\sigma^2c$ ,  $\hat{C}_0 = \frac{\pi(\sqrt{X_{(n)}} - \sqrt{X_{(1)}})^2}{2}$ , we have

$$\begin{aligned}
\int_a^b |\hat{p}(x) - p(x)| dx &= \int_a^b \left| \frac{\sqrt{(b-x)(x-a)}}{C_0 x} - \frac{\sqrt{(X_{(n)}-x)(x-X_{(1)})}}{\hat{C}_0 x} I([X_{(1)}, X_{(n)}]) \right| dx \\
&\leq \int_a^b \left| \frac{1}{\hat{C}_0} \right| \cdot \left| \frac{\sqrt{(b-x)(x-a)}}{x} - \frac{\sqrt{(X_{(n)}-x)(x-X_{(1)})}}{x} I([X_{(1)}, X_{(n)}]) \right| dx \\
&\quad + \left| \frac{1}{C_0} - \frac{1}{\hat{C}_0} \right| \triangleq P_1 + P_2,
\end{aligned}$$

note that  $\hat{C}_0 \xrightarrow{p} C_0 > 0$ , by continuous mapping,  $\frac{1}{\hat{C}_0} \xrightarrow{p} \frac{1}{C_0} > 0$ , thus  $\frac{1}{\hat{C}_0} = O_P(1)$ .

For the second part  $P_2 = \left| \frac{1}{C_0} - \frac{1}{\hat{C}_0} \right|$ , we have

$$\begin{aligned}
\left| \frac{1}{C_0} - \frac{1}{\hat{C}_0} \right| &= \frac{\pi((\sqrt{b} - \sqrt{a})^2 - (\sqrt{X_{(n)}} - \sqrt{X_{(1)}})^2)}{2C_0\hat{C}_0} \\
&\leq O_P(1) \cdot O_P(\sqrt{b} - \sqrt{X_{(n)}} + \sqrt{X_{(1)}} - \sqrt{a}) \\
&= O_P(n^{-\frac{2}{3}}),
\end{aligned}$$

for the first part, the integration can be separated as

$$P_1 = \int_a^{X_{(1)}} \cdot + \int_{X_{(1)}}^{X_{(n)}} \cdot + \int_{X_{(n)}}^b \cdot \\ \triangleq P_{11} + P_{12} + P_{13},$$

$$P_{11} = p(x^*)(X_{(1)} - a) = O_P(n^{-\frac{2}{3}}),$$

similar to get

$$P_{13} = p(x^*)(b - X_{(n)}) = O_P(n^{-\frac{2}{3}}),$$

$$P_{12} = O_P\left(\int_{X_{(1)}}^{X_{(n)}} \left| \frac{(b-a-X_{(n)}+X_{(1)})x-ab+X_{(n)}X_{(1)}}{x(\sqrt{(b-x)(x-a)}+\sqrt{(X_{(n)}-x)(x-X_{(1)})})} \right| dx\right) \\ = O_P\left(\int_{X_{(1)}}^{X_{(n)}} \left| \frac{b-a-X_{(n)}+X_{(1)}}{\sqrt{(b-x)(x-a)}} \right| dx\right) + O_P\left(\int_{X_{(1)}}^{X_{(n)}} \left| \frac{ab-X_{(n)}X_{(1)}}{x\sqrt{(b-x)(x-a)}} \right| dx\right),$$

by simple integration calculation, we have

$$P_{12} = O_P(n^{-\frac{1}{3}}).$$

Thus,

$$\int_a^b |\hat{p}(x) - p(x)| dx = O_P(n^{-\frac{1}{3}}),$$

which proves the proposition.

## D Algorithm

---

**Algorithm 1** Auto Detection of spikes

---

**Require:** Eigenvalues  $\{\lambda_i\}_{i=1}^N$ ,  $\alpha \leftarrow 7$ .  
Sort  $\lambda_i$  with descending order,  $\lambda_i > \lambda_{i+1}$   
**for**  $i = 1; i < N; i ++$  **do**  
     $\beta_i \leftarrow \lambda_i - \lambda_{i+1}$   
**end for**  
 $\beta = \sum_{i=1}^{N-1} \beta_i / (N - 1)$   
 $r \leftarrow \alpha \cdot \beta$   
**for**  $i = 1; i < N/2; i ++$  **do**  
    **if**  $\beta_i > r$  **then**  
        HS  $\leftarrow i$   
    **end if**  
**end for**  
**for**  $i = N - 1; i > N/2; i --$  **do**  
    **if**  $\beta_i > r$  **then**  
        TS  $\leftarrow N - i$   
    **end if**  
**end for**  
**return** HS,TS

---

The Algorithm 1 gives us an automatic method of detecting spikes, without the spike eigenvalues, we could achieve the deviation measurement between ESDs in weight matrices and standard MP Law by Algorithm 2.

---

**Algorithm 2** Get deviation measurement  $\hat{s}_n$ 

---

**Require:** Eigenvalues  $\{\lambda_i\}_{i=1}^N$ ,  $\alpha \leftarrow 7$ .

Sort  $\lambda_i$  with descending order,  $\lambda_i > \lambda_{i+1}$

HS,TS  $\leftarrow$  Algorithm 1( $\{\lambda_i\}_{i=1}^N$ ,  $\alpha$ )

$n \leftarrow N - \text{HS} - \text{TS}$

**for**  $i = 1; i \leq n; i++$  **do**

$\gamma_i \leftarrow \lambda_{i+\text{HS}}$

▷ Get eigenvalues lying in the bulk

**end for**

$M \leftarrow 2 \lfloor n^{\frac{1}{3}} \rfloor$

▷ The number of Bins

$H \leftarrow \lfloor n/M \rfloor$

$f(x) \leftarrow \frac{2\sqrt{(\gamma_1-x)(x-\gamma_n)}}{\pi(\sqrt{\gamma_1}-\sqrt{\gamma_n})^2x}$

$\hat{s}_n = 0$

**for**  $i = 1; i < M; i++$  **do**

$a, b \leftarrow (i-1)H + 1, iH + 1$

$L \leftarrow (b-a)/n/(\gamma_a - \gamma_b)$

$s \leftarrow \int_{\gamma_b}^{\gamma_a} |f(x) - L| dx$

$\hat{s}_n \leftarrow \hat{s}_n + s$

**end for**

$a, b \leftarrow (M-1)H + 1, n$

$L \leftarrow (b-a)/n/(\gamma_a - \gamma_b)$

$s \leftarrow \int_{\gamma_b}^{\gamma_a} |f(x) - L| dx$

$\hat{s}_n \leftarrow \hat{s}_n + s$

**return**  $\hat{s}_n$

---

## E spectral criterion with 0.6

**Table 12** Early stopping results in numeric experiments with  $C = 0.6$ : stopping epochs selected by spectral criterion in different layers' weight matrices and their testing accuracy (Test Acc). The symbol "-" means no early stopping epoch is found by the spectral criterion.

The combination NN1+ $\mathcal{D}_1$

Typical TP	spectral criterion $C = 0.6$				Final Epoch 248		
	epoch(FC2)	Test Acc	epoch(FC3)	Test Acc	FC1	FC2	Test Acc
0.15	8	24.58%	16	20.44%	HT	HT	20.17%
0.2	8	31.50%	16	25.83%	HT	HT	27.03%
0.3	8	49.09%	12	45.48%	HT	HT	44.80%
0.6	9	87.96%	-	-	MPB	MPB	88.30%
0.9	-	-	-	-	MP	MP	99.13%

The combination NN1+ $\mathcal{D}_2$

Typical TP	spectral criterion $C = 0.6$				Final Epoch 248		
	epoch(FC2)	Test Acc	epoch(FC3)	Test Acc	FC1	FC2	Test Acc
0.24	9	14.69%	-	-	HT	HT	13.08%
1.2	8	39.31%	16	32.11%	HT	HT	32.98%
2.4	8	76.75%	20	74.29%	HT	HT	75.92%
3.2	10	91.94%	-	-	HT	MPB	92.64%
4.8	-	-	-	-	MP	MP	99.73%

The combination NN2+ $\mathcal{D}_1$

Typical TP	spectral criterion $C = 0.6$				Final Epoch 248		
	epoch(FC1)	Test Acc	epoch(FC2)	Test Acc	FC1	FC2	Test Acc
0.02	-	-	-	-	HT	MPB	16.02%
0.04	-	-	-	-	HT	MPB	25.38%
0.07	-	-	-	-	HT	MPB	50.12%
0.13	-	-	-	-	MPB	MP	87.50%
0.2	-	-	-	-	MP	MP	99.14%

The combination NN2+ $\mathcal{D}_2$

Typical TP	spectral criterion $C = 0.6$				Final Epoch 248		
	epoch(FC1)	Test Acc	epoch(FC2)	Test Acc	FC1	FC2	Test Acc
0.24	12	13.48%	7	13.19%	HT	HT	13.44%
1.2	24	35.80%	5	34.63%	HT	HT	36.31%
2.4	6	73.80%	36	74.86%	MPB	MPB	75.12%
3.2	-	-	-	-	MP	MP	91.20%
4.8	-	-	-	-	MP	MP	99.59%

**Table 13** Early stopping results in real data experiments with  $C = 0.6$ .

## The combination LeNet+MNIST

batchsize	spectral criterion $C = 0.6$				Final Epoch 248		
	epoch(FC1)	Test Acc	epoch(FC2)	Test Acc	FC1	FC2	Test Acc
16	-		32	99.19%	MP	MPB	99.17%
32	-		-		MP	MPB	99.17%
64	-		-		MP	MPB	98.98%
128	-		-		MP	MP	99.03%
256	-		-		MP	MP	98.96%

## The combination LeNet+CIFAR10

batchsize	spectral criterion $C = 0.6$				Final Epoch 248		
	epoch(FC1)	Test Acc	epoch(FC2)	Test Acc	FC1	FC2	Test Acc
16	28	61.66%	8	61.62%	MPB	HT	64.99%
32	-		20	61.06%	MP	HT	64.57%
64	-		32	60.27%	MP	HT	62.49%
128	-		60	61.38%	MP	HT	61.83%
256	-		92	58.33%	MP	HT	60.49%

## The combination MiniAlexNet+MNIST

batchsize	spectral criterion $C = 0.6$				Final Epoch 248		
	epoch(FC1)	Test Acc	epoch(FC2)	Test Acc	FC1	FC2	Test Acc
16	5	98.64%	-		MPB	MP	99.49%
32	-		-		MP	MP	99.41%
64	-		-		MP	MP	99.42%
128	-		-		MP	MP	99.39%
256	-		-		MP	MP	99.31%

## The combination MiniAlexNet+CIFAR10

batchsize	spectral criterion $C = 0.6$				Final Epoch 248		
	epoch(FC1)	Test Acc	epoch(FC2)	Test Acc	FC1	FC2	Test Acc
16	4	71.01%	36(RC)	55.6%	HT	RC	10%(explode)
32	4	72.17%	196(RC)	62.84%	HT	RC	10%(explode)
64	6	73.03%	-		HT	MP	77.94%
128	12	74.31%	-		HT	MP	77.43%
256	28	75.87%	-		MPB	MP	75.93%